L81 2nd pages / 1 of 19

Pliocene intraplate-type volcanism in the Andean foreland at 26°10′S, 64°40′W (NW Argentina): Implications for magmatic and structural evolution of the Central Andes

A. Gioncada[1], L. Vezzoli[2], R. Mazzuoli[1], R. Omarini[3], P. Nonnotte[4], and H. Guillou[5]

[1]DIPARTIMENTO DI SCIENZE DELLA TERRA, UNIVERSITÀ DI PISA, VIA S. MARIA 53, 56126 PISA, ITALY

[2]DIPARTIMENTO DI SCIENZE CHIMICHE E AMBIENTALI, UNIVERSITÀ DELL'INSUBRIA, VIA VALLEGGIO 11, 22100 COMO, ITALY

[3]FACULTAD DE CIENCIAS NATURALES, UNIVERSIDAD NACIONAL DE SALTA, CONSEJO NACIONAL DE INVESTIGACIONES CIENTÍFICAS Y TÉCNICAS (CONICET), AVENIDA BOLIVIA Nº 5150, CP 4400, SALTA, ARGENTINA

[4]UNIVERSITÉ EUROPÉENNE DE BRETAGNE, FRANCE, AND UNIVERSITÉ DE BREST, CNRS, UMR 6538 DOMAINES OCÉANIQUES, INSTITUT UNIVERSITAIRE EUROPÉEN DE LA MER, PLACE N. COPERNIC, 29280 PLOUZANÉ, FRANCE

[5]COMMISSARIAT À L'ENERGIE ATOMIQUE/CENTRE NATIONAL DE LA RECHERCHE SCIENTIFIQUE (CEA-CNRS), UMR 1572, LABORATOIRE DES SCIENCES DU CLIMAT ET DE L'ENVIRONNEMENT, DOMAINE DU CNRS BÂTIMENT , AVENUE DE LA TERRASSE, 91198 GIF SUR YVETTE, FRANCE

ABSTRACT

The Antilla magmatic complex (26°10′S, 64°40′W, NW Argentina) attests to magma eruption at ca. 4.7 Ma in the Central Andes backarc region, 300 km E of the active arc. The Antilla lavas have an alkaline, predominantly mafic composition and record the most primitive isotopic ratios ($^{87}Sr/^{86}Sr$ = 0.704360 and $^{143}Nd/^{144}Nd$ = 0.512764) of Central Andes Neogene backarc volcanism between 24°S and 27°S. They show trace-element patterns recalling backarc Pliocene-Quaternary intraplate mafic rocks, but they show lower silica and higher alkali contents, and are interpreted to derive from the depleted subcontinental mantle.

A revision of the structural and volcanological characteristics of the Central Andes between 24°S and 27°S shows that this region was, during the Miocene-Pliocene, the site of lithospheric processes that account for partial melting in the mantle wedge, in the subcontinental mantle, and in the continental crust. The existing geophysical and petrological data agree with a model in which magma production was related to a process of lithospheric delamination. The Antilla rocks are the easternmost volcanic products with intraplate characteristics, located beside a large zone of partial melting of the continental crust, at the intersection of the NW-trending Archibarca and NE-trending Tucumán transversal lineaments. Their age of 4.7 Ma corresponds to the acme of mafic monogenetic and silicic ignimbrite volcanism in the backarc at the same latitude. This provides new constraints for the spatial and temporal reconstruction of deformation events in the crust and of the lithospheric delamination process and its bearing on magmatic activity.

LITHOSPHERE; v. 2; no. X; p. 1–19. doi: 10.1130/L81.1

INTRODUCTION

In the Central Andes, long-lived Jurassic to present subduction has led to a complex magmatic and tectonic evolution and to substantial modifications of the lithospheric mantle and crust. The Miocene to present magmatic arc is linked to the subduction of the Nazca plate under the South America continent, and it forms a continuous N-S–striking belt of calc-alkaline volcanoes and calderas representing the Western Cordillera (Fig. 1). Behind the arc, between 24°S and 27°S, magmatic belts have developed eastward for ~300 km from the active arc across the 4000-m-high Puna Plateau. These magmatic belts are connected to NW-SE–trending strike-slip fault systems (Lipez, Calama–Olacapato–El Toro, Archibarca, Culampaja, and Ojos del Salado fault systems; Fig. 1) (Coira et al., 1993; Riller et al., 2001; Matteini et al., 2002; Chernicoff et al., 2002; Acocella et al., 2007). Volcanic centers in backarc position (i.e., Farallón Negro [Sasso and Clark, 1998]; Portezuelo de Las Animas [González et al., 2005]; Antilla [Viramonte et al., 1994a]) are also present along the NE-trending Tucumán transfer zone (Fig. 1; de Urreiztieta et al., 1996). The whole history of volcanic activity in the backarc region is an important indicator of the time-space evolution of the Andean orogens, and, therefore, it plays a fundamental role in the reconstruction of the thermal and compositional state of the upper mantle and lithosphere and of the tectonic history of the upper crust.

The backarc magmatic products between 24°S and 27°S show different geochemical characteristics, in terms of both isotopic ratios and trace-element composition, indicating different sources involved in magma genesis and complex processes responsible for their origin (e.g., Kay et al., 1994; Matteini et al., 2002; Petrinovic et al., 2005; Mazzuoli et al., 2008). Moving from the active arc (Western Cordillera) to the Eastern Cordillera (Fig. 1), the geochemical magma signature changes from typical calc-alkaline to crustal to intraplate (Kay et al., 1994; Mazzuoli et al., 2008). Recently, different isotopic compositions determined in backarc lithospheric magmas have suggested the existence of different chemical domains in the subcontinental lithospheric mantle (Mazzuoli et al., 2008; Drew et al., 2009). Most reconstructions based on geophysical and petrological data refer to a piecemeal lithosphere delamination process leading to thinning of lithospheric mantle and consequent ascent and melting of asthenosphere, which in turn induces partial melting of lower and upper crust and lithosphere mantle itself (Kay et al., 1994; Mazzuoli et al., 2008; Drew et al., 2009). Although models invoking lithospheric loss can reconcile the genesis of magmas from different sources, the crustal deformation, and the uplift of the Puna Plateau, our understanding of the geodynamic forces that drive these regional-scale events remains incomplete. Some of the major topics to address in order to understand the general and specific processes of magma genesis and

For permission to copy, contact editing@geosociety.org | © 2010 Geological Society of America

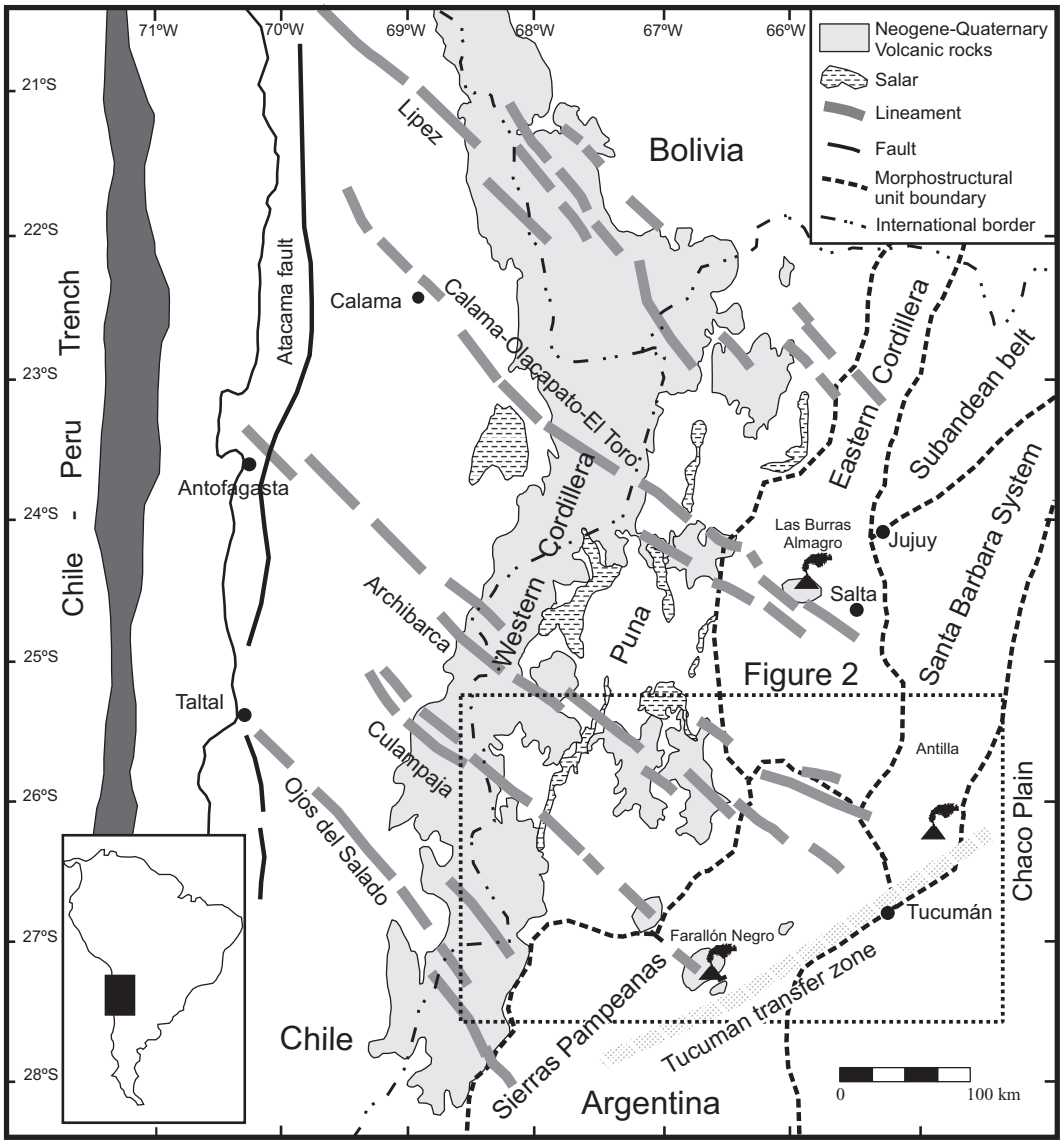

Figure 1. Regional geologic sketch map of the Central Andes between 21°S and 28°S, showing the main morphostructural units, the location of transversal lineaments, and the extent of the Miocene to present-day volcanism in the main arc (Western Cordillera) and backarc regions. Inset shows the location on the South America map. The Las Burras–Almagro (Mazzuoli et al., 2008), Antilla (this study), and Farallón Negro (Sasso and Clark, 1998) magmatic complexes lie at the eastern edge of the Calama–Olacapato–El Toro, Archibarca, and Culumpaja NW-trending fault zones, respectively. Box is the location of Figure 2.

evolution in the Central Andes backarc magmatism are: (1) the nature and structure of the subcontinental lithospheric mantle and its role in the generation of magmas, particularly in the easternmost sector of the backarc, and (2) the role of deformation of the crust in magma transport, shallow storage, and ascent to the surface. The present research was conducted in an attempt to provide a solution to these questions by studying backarc products very far from the trench.

Our study is focused on a small magmatic complex, dispersed over a 150 km^2 area near the village of Antilla (26°10′S, 64°40′W, Salta Province, NW Argentina), ~650 km from the Pacific trench (Figs. 1 and 2). The Pliocene Antilla magmatic complex, mainly formed of mafic rocks (Viramonte et al., 1994a), is located in a key area at the boundary of the morphotectonic units of the Eastern Cordillera, Sierras Pampeanas, and Santa Barbara System and at the intersection of the NW-trending Archibarca fault zone with the NE-trending Tucumán lineament (Figs. 1 and 2). This work presents a new geologic field survey, K/Ar chronology, and geochemical, petrological, and isotopic data on the Antilla rocks with the purpose of discussing the petrogenesis and tectonic setting of this volcanism in a regional geologic context, by comparing the Antilla rocks with those of Miocene-Pliocene age set in the southern Puna Plateau. Although these new data focus on a small volcanic center far from the active arc, they are of great importance for characterizing the lithospheric mantle in the backarc, and they contribute to define the limits, in space and time, of lithospheric delamination, one of the most important geological events controlling the evolution of Central Andes in the past 15 Ma.

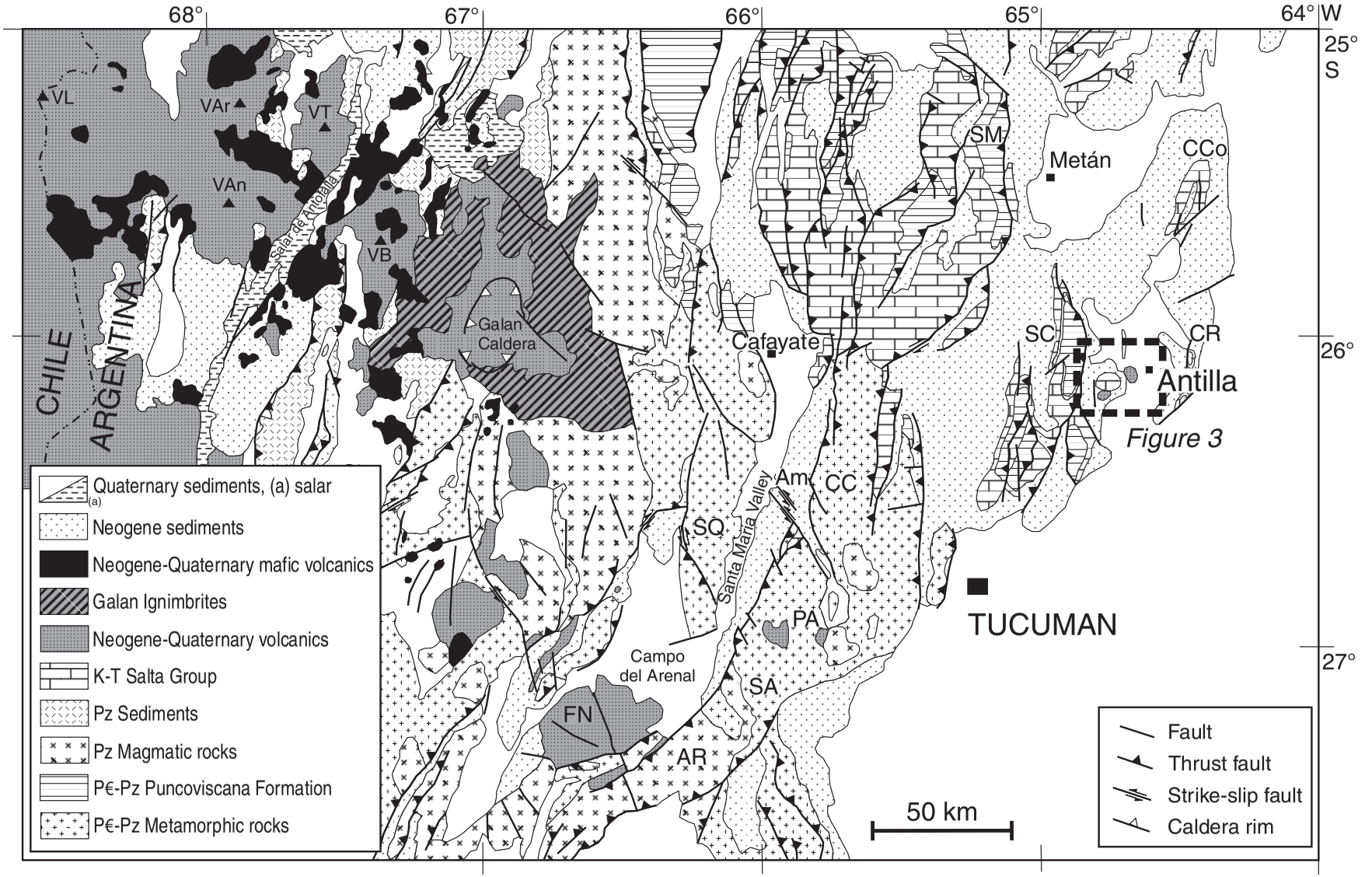

Figure 2. Geologic map of the Central Andes between 25°S and 28°S along the Archibarca lineament from the main arc (Western Cordillera) to the front of the deformed foreland, based upon new geologic mapping, Landsat image interpretation, and previously published map of Allmendinger et al. (1983) and Kraemer et al. (1999). Am—Amaicha, AR—Aqua Rica, CC—Cunbre Calchaquies, CCo—Cerro Colorado, CR—Cerro Remate, FN—Farallón Negro, PA—Portozuelo de Las Animas, SA—Sierra del Aconquija, SC—Sierra de la Candelaria, SM—Sierra de Metan, SQ—Sierra de Quilmes, VAn—Volcano Antofalla, VAr—Volcano Archibarca, VB—Volcano Beltran, VL—Volcano Lastarria, VT—Volcano Tebenquicho. Box shows the location of the mapped area in Figure 3.

L81 2nd pages / 4 of 19

CENTRAL ANDES AT 26°S

Regional Geologic Setting

The Central Andes at ~26°S represent the southern part of the transition zone developing between the 30°-dipping (N of 24°S) and the subhorizontal (S of 27°30′S) sections of the Nazca plate slab (Cahill and Isacks, 1992). In recent years, the application of high-precision geophysical techniques (see Prezzi et al., 2009, and references therein) has significantly influenced the new tectonic models for this sector. At present, the weight of evidence clearly supports the architecture of the transition zone as oblique (SW-NE), approximately coincident with the direction of the Tucumán transfer zone. This configuration of the subducting Nazca plate is interpreted to be responsible for the major structural differences in the style of foreland deformation, in conjunction with inherited paleogeographic (Grier et al., 1991; Marquillas et al., 2005) and structural (Allmendinger et al., 1983) pre-Andean features.

The Eastern Cordillera is a basement-involved fold-and-thrust system with bivergent, N-S– to NE-striking thrust faults (Kley et al., 1996; Mon, 1999), and it is characterized by a low-grade metamorphosed Proterozoic–early Paleozoic basement (Puncoviscana Formation; Omarini et al., 1999) that is unconformably covered by a thick Paleozoic sedimentary sequence. In the southern Eastern Cordillera, Paleozoic rocks are absent, and the well-developed Cretaceous–Paleogene Salta Group strata were deposited directly on the basement (Fig. 2). In this region, the NNE-SSW–striking and W-dipping frontal thrust-fault system of the Eastern Cordillera represents a main border fault of the Cretaceous rift that was reactivated by inversion during the Cenozoic (Carrera et al., 2006; Carrera and Muñoz, 2008), and it poses a basement slice (Sierra de Metán) over the Cenozoic sediments of the Metán Basin with a thrust offset of ~10–15 km (Fig. 2) (Mon et al., 2005). East of this frontal thrust, a structural high belonging to the Santa Barbara System (Cerro Colorado; Fig. 2) shows exposures of Paleozoic units and an eastward thickness reduction of the Salta Group strata (Mon et al., 2005).

The Santa Barbara System (Kley and Monaldi, 1999) is a fold-and-thrust belt harmonically involving Proterozoic, lower Paleozoic (Ordovician-Devonian), Cretaceous-Paleogene (Salta Group), and Cenozoic (Orán Group) units. In the area of interest, the Santa Barbara System coincides with a NE-SW–trending branch of the Cretaceous continental rift, with a depocenter in the Metán Basin (González and Mon, 1996; Kley and Monaldi, 1999; Mon et al., 2005). The pre-Cretaceous basement, composed of Proterozoic–early Paleozoic highly microfolded metapelites, is exposed at the core of asymmetric anticlines forming laterally discontinuous, subparallel ranges of moderate topography with frequent and abrupt changes of strike from N-S to NE-SW (Fig. 2) (Allmendinger et al., 1983; González and Mon, 1996; Kley et al., 1999). The anticline-bounding faults were extensional normal faults bordering the Cretaceous rift basin that were inverted during the Andean orogeny (Cristallini et al., 1997; Kley and Monaldi, 2002). They dip both to SE and NW following the original geometry of rift-related faults. Across these faults, pre-Neogene sediments record an abrupt change of thickness and lithofacies (Mon et al., 2005). Several NE-striking reverse faults show a dextral, strike-slip component (Fig. 2). The Cenozoic sequence (Orán Group) is well developed and covers the Salta Group with a low-angle unconformity (Mingramm et al., 1979).

The Sierras Pampeanas consist of spatially isolated, N-trending crystalline basement blocks that are uplifted along NNE-striking reverse faults and that overthrust Neogene and Quaternary sediments of intermontane basins (Mon, 1976, 1979; Jordan and Allmendinger, 1986; González and Mon, 1996). In the northernmost Sierras Pampeanas ranges (Sierra de Quilmes, Sierra del Aconquija, and Cumbres Calchaquies; Fig. 2), the crystalline basement consists of Upper Proterozoic and/or lower Paleozoic rocks metamorphosed from upper greenschist to amphibolite facies, sometimes migmatized, and intruded by lower Paleozoic granitoids. The upper Paleozoic and Mesozoic sequences are lacking. The Cretaceous units related to the Salta rift thin westward and disappear on the eastern flank of the Cumbres Calchaquies. The Neogene–Quaternary strata unconformably overlie a basement peneplain surface that formed in the Late Cretaceous due to the denudation of the rift shoulders (Allmendinger et al., 1983; Coughlin et al., 1998; Sobel and Strecker, 2003). The Neogene–Quaternary sediments filled the intermontane basins (Coutand et al., 2001, 2006; Mortimer et al., 2007) and are well represented by the stratigraphic sequence of the Santa Maria Valley (Bossi et al., 2001).

The southern Puna (Allmendinger, 1986; Allmendinger et al., 1989; Marrett et al., 1994) has two distinct basement sequences (Fig. 2). The western part of the Puna Plateau is characterized by elongated fault-bounded ranges of Paleozoic sedimentary strata (Ordovician) folded along N-S axes and intervening, internally drained basins (salars). In the eastern part, the crystalline basement consists of amphibole-grade metasedimentary strata of Proterozoic or early Paleozoic age with granitoid intrusions similar to the basement of the Sierras Pampeanas (Siebel et al., 2001). Neogene–Quaternary andesitic to dacitic volcanic sequences unconformably mantle older deposits and are poorly deformed (Fig. 2). At the southeastern border of the Puna, transitional with the Sierras Pampeanas, the Neogene sedimentary and volcanic sequence spans from ca. 11 Ma to 2.3 Ma, without evidence of internal unconformities, and rests directly on the crystalline basement (Strecker et al., 1987; Allmendinger et al., 1989). The Miocene rocks are transitional to or unconformably overlain by a boulder conglomerate (Punaschotter Formation; Allmendinger, 1986) of probable Pliocene age (3.8 Ma; Carrapa et al., 2008).

Elements and Timing of Upper-Crust Deformation

The Puna Plateau and the eastern Andean foreland region at ~26°S show three prominent regional structural trends running about N-S, NE-SW, and NW-SE, parallel and transversal, respectively, to the main direction of the orogenic structures.

The major N- to NNE-trending set corresponds to the regional-scale thrust faults of the Eastern Cordillera and northern Sierras Pampeanas and to the fold axes of the Paleozoic ranges in the Puna Plateau (Fig. 2). These thrusts were reactivated during Neogene as sinistral transtensional strike-slip faults, determining the major NNE-elongated salar depressions (i.e., Salar de Antofalla; Fig. 2; Kraemer et al., 1999; Coutand et al., 2001).

The NW- and NE-trending transverse systems cut across the Puna Plateau and the eastern foreland provinces of the Eastern Cordillera and Sierras Pampeanas (Figs. 1 and 2). During the Neogene, the NW- and NE-trending faults formed conjugate systems (Allmendinger, 1984; Strecker et al., 1989; Assumpção and Araujo, 1993) and had sinistral and dextral motion, respectively, consistent with dominant regional E-W shortening (Allmendinger et al., 1983). Many of these transverse lineaments were active prior to the Cenozoic and are interpreted to represent crustal structures, compositional anisotropies in the lithosphere, and/or pre-Andean paleogeographic boundaries, exerting an important influence on regional tectonic style.

At ~26°S, the NW-striking Archibarca lineament develops (Fig. 1). On the Puna Plateau, NW-striking faults can be traced discontinuously and are obscured by Neogene–Quaternary volcanic cover, whereas they are more evident on the southeastern Puna border, Sierras Pampeanas, and Santa Barbara System (Fig. 2) (Allmendinger, 1984, 1986).

The NE-striking Tucumán lineament (Mon, 1976; Allmendinger et al., 1983) was defined by de Urreiztieta et al. (1996) as a dextral transpressional

transfer zone accommodating the lateral decrease in amounts of bulk horizontal shortening and crustal thickening occurring at ~27°S. Along this lineament, a horizontal offset of ~350 km was produced between the main deformation front of the Subandean foreland provinces to the north and the Precordillera to the south (Fig. 1). It also coincides with structural and stratigraphic regional boundaries between the Puna Plateau and Eastern Cordillera and Santa Barbara System (Figs. 1 and 2). The Tucumán lineament is 100 km wide, can be followed for at least 350 km (Fig. 1), and appears as a broad diffuse zone of distributed right-lateral shearing rather than strike-slip faulting along discrete faults (Allmendinger, 1984; Allmendinger et al., 1989; de Urreiztieta et al., 1996). Notwithstanding these factors, several NE-striking faults of the Sierras Pampeanas and Santa Barbara System show a dextral strike-slip component (de Urreiztieta et al., 1996) (Fig. 2).

The onset and evolution of Cenozoic deformation along the transect at ~26°S have been recently constrained by apatite fission-track thermochronology on uplifted blocks of the Eastern Cordillera and Sierras Pampeanas (Coutand et al., 2001, 2006; Sobel and Strecker, 2003; Deeken et al., 2006; Mortimer et al., 2007; Carrapa et al., 2008). Along this transect, timing of the upper-crustal deformation becomes more recent eastward. In the southern Puna Plateau, the last significant compressive deformation occurred during the middle to late Miocene (<15 Ma; Vandervoort et al., 1995). Uplift of the Sierras Pampeanas ranges is interpreted to have started at ca. 6 Ma (Strecker et al., 1989; Sobel and Strecker, 2003; Carrapa et al., 2008). In the Santa Maria Basin, the sediments do not record any evidence for tectonic deformation until ca. 7 Ma (Kleinert and Strecker, 2001). Two phases of deformation are recorded by the Neogene–Quaternary sequence of this basin, both with WNW-ESE shortening and subvertical extension along thrust faults. Similarly, at the southeastern border of the Puna, at the transition with the Sierras Pampeanas, two phases of late Cenozoic deformation are stratigraphically separated by the deposition of the boulder conglomerate of the Punaschotter Formation (Allmendinger, 1986; Allmendinger et al., 1989; Carrapa et al., 2008). The first phase started between 10 and 5 Ma and is older than 3.53 Ma (Allmendinger, 1984, 1986; Trumbull et al., 2006). The younger phase produced normal, reverse, NE-striking right-lateral, and NW-striking left-lateral strike-slip faults. On the Santa Barbara System (Carrera and Muñoz, 2008), a first deformation event is recorded by the decrease in thickness of the Guanaco Formation (10–5 Ma) across the crest of anticlinal folds (Reynolds et al., 1994; Gomez Omil and Albarino, 1996), and the main phase of deformation developed during the deposition of the Piquete Formation since ca. 5 Ma.

Time-Space Distribution and Characteristics of Backarc Magmatism

In the Central Andes between 24°S and 27°S, late Miocene–Quaternary backarc magmatism was focused in the southern Puna Plateau and Eastern Cordillera along NW-trending lineaments (Calama–Olacapato–El Toro, Archibarca, and Culumpajá) and in the northern Sierras Pampeanas along the NE-trending Tucumán lineament (Figs. 1 and 2).

The backarc volcanism in the southern Puna, along the Calama–Olacapato–El Toro and Archibarca fault systems, was characterized by three different volcanic kinds: stratovolcanoes, ignimbrites, and small mafic centers (Coira et al., 1982, 1993; Allmendinger et al., 1997), and sporadically by intrusive massifs. Along the Calama–Olacapato–El Toro, the products of some Miocene stratovolcanoes have been interpreted as deriving by partial melting of lower crust (Matteini et al., 2002). Along the easternmost portion of the same lineaments, Miocene intrusive and volcanic rocks with intraplate signature were emplaced (La Burras–Almagro–El Toro magmatic complex; Mazzuoli et al., 2008). Along the Archibarca lineament, the middle Miocene–Pliocene andesitic to dacitic stratovolcanoes exhibit a calc-alkaline signature with a higher degree of crustal contamination than the andesite-dacite lavas of the frontal arc (Western Cordillera) (Coira and Pezzutti, 1976; Coira et al., 1993; Kay et al., 1999; Kraemer et al., 1999; Richards et al., 2006). It is worth noting that these stratovolcanoes have an extraordinary long-lived history, spanning 6–9 Ma (Risse et al., 2008), compared to the normal evolution of such kind of volcanoes. Small-volume, rhyolitic ignimbrites, middle Miocene–Pliocene in age (11–4 Ma; Siebel et al., 2001), show an isotopic composition similar to that of the stratovolcanoes of the frontal arc. They are interpreted as products of crystal fractionation of magmas similar to the contemporaneous subduction-related andesites, with little intervention of crustal contamination (Coira et al., 1993; Siebel et al., 2001; Schnurr et al., 2007). Contemporaneously, the Cerro Galan caldera outpoured dacitic, crystal-rich, large-volume ignimbrites (Fig. 2) with geochemical and isotopic signatures (Francis et al., 1980, 1989; Sparks et al., 1985) that provide evidence for large-scale intracrustal melting with a minor mantle component, similar to the ignimbrite flare-ups of the Altiplano-Puna volcanic complex (de Silva, 1989). Mafic volcanism (mainly basaltic andesite and andesite) formed small, scattered, monogenetic cinder and spatter cones and fissures with associated low-volume lava flows (Fig. 2) during the late Miocene–Pleistocene (Coira et al., 1982, 1993; Knox et al., 1989; Kay et al., 1994, 1997, 1999; Kraemer et al., 1999; Risse et al., 2008). Based on their geochemical characteristics, the products of the mafic backarc centers have been distinguished into K-rich calc-alkaline, shoshonite, and intraplate, reflecting their different mantle sources (Kay et al., 1994).

The onset of the backarc mafic volcanism in the southern Puna occurred at 7.3 Ma and reached a maximum of activity at 5.3–3.6 Ma (Kay et al., 1999; Kraemer et al., 1999; Risse et al., 2008; Drew et al., 2009). Volcanic activity continued with some fluctuations through the Pleistocene. The main phases of mafic backarc volcanism coincided with the waning activity of backarc stratovolcanoes (Risse et al., 2008). Moreover, there is a correspondence in time between the peak of mafic volcanism and the major silicic ignimbrite eruptions of the Cerro Galan caldera (Sparks et al., 1985; Francis et al., 1983).

Miocene magmatism in the northern Sierras Pampeanas is represented by the Farallón Negro and Agua Rica volcanic centers, and the andesitic breccias and lavas of the Portozuelos de las Animas on top of Sierra del Aconquija (Figs. 1 and 2). At Farallón Negro, basalts and basaltic andesites were erupted between 12.5 and 8.5 Ma, and an andesitic stratovolcano was active between 8.5 and 7.5 Ma (Sasso and Clark, 1998). The youngest phase of magmatic activity in the Farallón Negro was the intrusion of a NW-trending dacite and rhyolite dike swarm between 7 and 5.1 Ma (Caelles et al., 1971; Sasso and Clark, 1998). The Agua Rica center includes a monzonitic intrusive complex emplaced at 8.6 Ma and younger andesite porphyry mineralized at 5.4 Ma (Sasso and Clark, 1998). The Portozuelos de las Animas volcanism is inferred to have been active between 11.6 and 7.7 Ma (González et al., 2005).

The only volcanic activity in the Santa Barbara System is the Antilla magmatic complex, the study of which is presented in this paper.

System at Depth: Crust, Lithosphere, and Upper Mantle

The thickness of the crust and lithospheric mantle and the depth of the subducted slab are critical constraints for geodynamic models on Andean structural evolution and genesis of backarc magmatism. Currently, the continental crust thickness estimated beneath southern Puna and Eastern Cordillera at ~25°S is 42–59 km, with an irregular distribution and a southward decreasing trend (Yuan et al., 2002; McGlashan et al., 2008, and references therein). Across the transect of the Central Andes at 26°S,

lithosphere thickness is modeled at 60 km beneath the southern Puna Plateau and 90–100 km eastward beneath the transitional area with the Sierras Pampeanas and Santa Barbara System (Whitman et al., 1992, 1996). Across the same transect at 26°S, the subducting Nazca slab is 90–100 km deep beneath the Western Cordillera and 300 km deep beneath the Antilla magmatic complex (Cahill and Isacks, 1992).

Geophysical data in the southern Puna, with strong seismic attenuation, low P- and S-wave velocities, and high electrical conductivity (Whitman et al., 1992; Yuan et al., 2000; Schurr et al., 2003; Koulakov et al., 2006; Asch et al., 2006), indicate anomalously high temperatures and the presence of partial melts in the midcrust at ~20–25 km depth beneath the Galan caldera region, similar to the Altiplano-Puna volcanic complex.

The crustal thinning, high elevation of ~4000 m, a felsic composition of the crust (Zandt et al., 1994; Beck and Zandt, 2002), the absence of a thick mantle lid (Whitman et al., 1996), the extensive crustal melting, and the mafic backarc magmatism (Kay et al., 1994; Risse et al., 2008) are features that have been interpreted to indicate the foundering of lower portions of the lithosphere (lithospheric delamination), replaced by an upflow of hot asthenosphere (Kay and Kay, 1993; Kay et al., 1994; Schurr et al., 2006; Kay and Coira, 2009).

ANTILLA MAGMATIC COMPLEX

Our work is focused on the Neogene magmatic rocks exposed near the village of Antilla (Salta Province, 26°10′S, 64°40′W, 550–750 m above sea level [asl]) in the southern part of the Subandean foreland province called the Santa Barbara System (Figs. 1, 2, and 3). This is the only and most eastern occurrence of Neogene backarc magmatism documented in this sector of the Andean foreland. Insight into the stratigraphy and structure of the Antilla rocks from surface exposure is limited because the area is covered by extensive scrub vegetation, shows scarce erosion, and was subjected to intensive ground leveling for agricultural purposes. The Antilla magmatic complex was first recognized by Viramonte et al. (1994a). Presently, it appears as a volcanic field of different, monogenetic lava vents rather than a central volcanic edifice, extending over an area of ~150 km^2 around the Cerro Negro, on the eastern side of the Sierra de la Candelaria. These volcanic rocks crop out as lava flows and feeder dikes interlayered and intruded within Neogene sedimentary deposits (Fig. 3; Table 1).

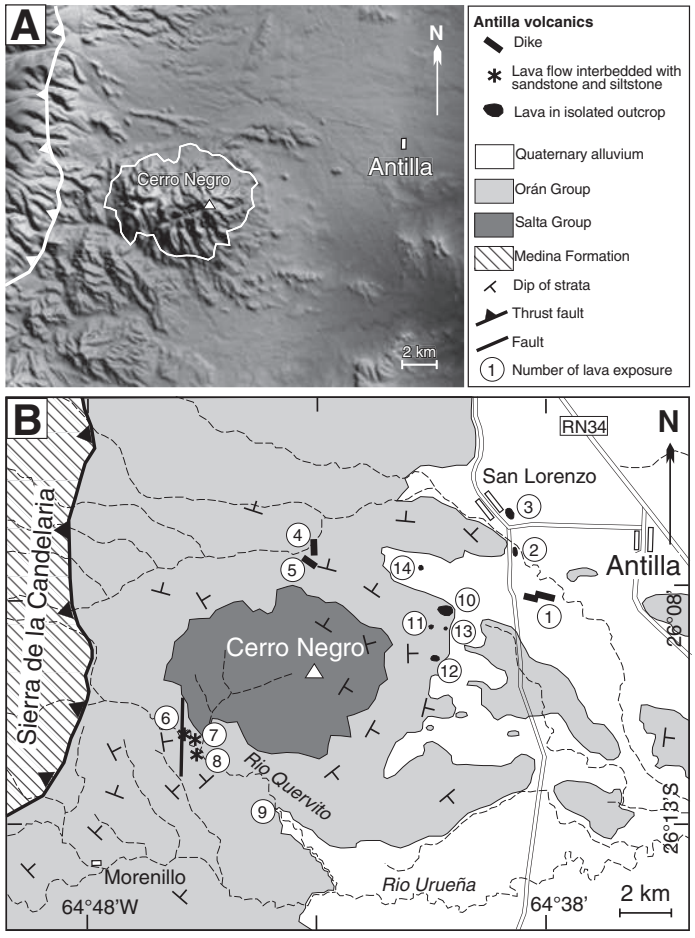

Figure 3. Shaded elevation model (A) and the detailed geologic map (B) of the Antilla magmatic complex. The area encompasses the eastern part of the Sierra de La Candelaria. Numbers refer to lava exposures as in Table 1.

Stratigraphy

In the study area, the crystalline basement forms the core of the anticline of Sierra de la Candelaria (Figs. 2 and 3) and is composed of medium-grade metamorphic rocks of the Medina Formation (Bossi, 1969). These microfolded schists probably represent the Proterozoic–early Paleozoic Puncoviscana Formation, but pervasive shearing that developed during the Early Cambrian deformational event has obscured the original lithofacies (Willner, 1990). The overlying Paleozoic sedimentary rocks show variable distribution and thickness. The Middle Cambrian Mesón Group is composed of fine-grained whitish and pinkish quartzite overlying the crystalline basement with angular unconformity in the Sierra de la Candelaria range. The conformable Ordovician Santa Victoria Group includes shallow-marine fossiliferous sandstone, mudstone, and shale (Aceñolaza, 1992). The overlying Silurian-Devonian strata are unconformable.

The Paleozoic sequence is unconformably overlain by the Cretaceous–Paleogene Salta Group (Figs. 2 and 3), coinciding in the study area with the Metán Basin, which includes two sedimentary stages. The first stage represents the infilling of a synrift basin and is represented by the Cretaceous–Campanian Pirgua Subgroup, including reddish conglomerates, sandstone, shale, and alkaline volcanic rocks (Marquillas and Salfity, 1988; Viramonte et al., 1999). Conglomerates of the basal Pirgua Subgroup overlie the Devonian quartzite at the core of the Cerro Colorado and Cerro Remate anticlines (Fig. 2). The conglomerate has a vertical and lateral transition to red and pink, massive quartz sandstone with interlayers of mudstone, as in the Cerro Negro anticline. The thickness of the Pirgua Subgroup is 1100 m in the Cerro Colorado and 3500 m in the central part of the Metán Basin. The second stage (Maastrichtian–Eocene) is related to the basin postrift infilling and includes the Balbuena and Santa Barbara Subgroups, both intruded by basaltic lavas and dikes (Viramonte et al., 1999). The Balbuena Subgroup is composed of basal massive calcareous sandstone (Lecho Formation) and white and yellow oolitic limestone (Yacoraite Formation), distributed uniformly over the entire area with maximum thickness of 200 m in the Cerro Colorado. The Santa Barbara Subgroup is represented only by the Mealla Formation, cropping out around the Cerro Colorado, which is composed of yellow and red sandstone with interlayers of calcareous sandstone and calcrete paleosols. The exposed sequence lacks the younger units of the subgroup.

The stratigraphy of the Cenozoic units in the Antilla area is poorly known. According to Reynolds et al. (2000), the reference sequence of the Neogene sediments is represented by the 5000-m-thick Orán Group

TABLE 1. MAIN LITHOLOGIC, STRATIGRAPHIC AND PETROGRAPHIC CHARACTERISTICS OF THE ANTILLA VOLCANIC ROCKS

No.*	Coordinates		Lithofacies	Stratigraphic relationship	Sample	Petrography†
1	26°08′25S	64°37′90W	WNW-striking dike	Isolated exposure	ANT1	Hbl+Aug *+Pl+Cpx* (phyllosilicates, Cal)
1	26°08′25S	64°37′90W	WNW-striking dike	Isolated exposure, cuts dike ANT1	ANT2	Hbl+Aug (zeolites,Cal)
1	26°08′25S	64°37′90W	WNW-striking dike	Isolated exposure, cuts dikes ANT1 and ANT2	ANT3	Hbl+Aug *+Pl+Cpx* (phyllosilicates, Cal)
1	26°08′25S	64°37′90W	WNW-striking dike	Isolated exposure	ANT4	Hbl+Aug+Fe-Ti ox *+Pl+Kfs+Ol+Ap*
2	26°07′29S	64°38′50W	NW-striking dike	Isolated exposure	ANT5	Intense alteration, only Aug+Hbl recognizable
2	26°07′29S	64°38′50W	NW-striking dike	Isolated exposure	ANT6	Hbl+Aug+Fe-Ti ox *+Pl*
2	26°07′29S	64°38′50W	NW-striking dike	Isolated exposure	ANT7	Hbl+Aug+Fe-Ti ox *+Pl* (zeolites, phyllosilicates, Cal)
3	26°06′28S	64°38′34W	Dike?	Isolated exposure	ANT8	Hbl+Aug+Fe-Ti ox *+Pl+Kfs+Ol+Ap*
3	26°06′28S	64°38′34W	Dike?	Isolated exposure	ANT9	Intense alteration, only Hbl+Aug recognizable
4	26°07′34S	64°43′06W	N-striking dike, thickness 40 cm	Intrudes red fine-grained sandstone and laminated green mudstone dipping N100°E/5°	ANT10	Intense alteration, only Hbl+Aug recognizable
5	26°07′57S	64°43′18W	N125°E-striking dike, thickness 50 cm	Intrudes pink laminated siltstone and stratified white oolitic limestone dipping N32°E/10°	ANT12	Hbl+Agt+Aug+pl+Fe-Ti ox *+Pl+Kfs+Cpx+Ap*
6	26°10′88S	64°45′93W	Lava flow, thickness 20 m, massive	Intercalated with red and orange laminated siltstone and sandstone dipping N90°E/3°	ANT13	Hbl+Aug+Agt+Pl+Fe-Ti ox *+Pl+Kfs+Cpx+Ap*
6	26°10′89S	64°45′93W	Lava flow	Beneath the lava of sample ANT13	ANT14	Hbl+Agt+Aug+Pl+Fe-Ti ox *+Pl+Kfs+Cpx+Ap*
7	26°10′89S	64°45′84W	Lava flow	Beneath the lava of sample ANT14	ANT15	Hbl+Aug+pl+Fe-Ti ox *+Pl+Kfs+Cpx+Ap*
7	26°10′89S	64°45′84W	Lava flow	Beneath the lava of sample ANT15	ANT16	Pl+Hbl+Fe-Ti ox *+Pl+Kfs+Cpx+Ap*
8	26°11′28S	64°45′56W	Lava flow, thickness 3 m, massive	Intercalated with red and green laminated siltstone dipping N44°W/6°	ANT17	Hbl+Agt+Aug+Pl+Fe-Ti ox *+Pl+Cpx+Bt+Ap+opaques*
9	26°12′42S	64°43′43W	Block of lava		ANT18	Pl+Hbl+Fe-Ti ox *+Pl+Kfs+Ol+Ap*
10	26°08′38S	64°40′06W	Dike?	Intrudes fine-grained sandstone with lenses of gypsum	ANT19	Hbl+Aug+Fe-Ti ox
11	26°08′90S	64°40′38W	Dike?	Intrudes fine-grained sandstone with lenses of gypsum	ANT20	Pl+ Hbl+Agt+Aug+Ttn *+Pl+Kfs+Cpx+Ap*
12	26°09′45S	64°40′32W	Dike?	Intrudes fine-grained sandstone with lenses of gypsum	ANT21	Pl+ Hbl+Agt+Aug+Ttn+Fe-Ti ox+ap *+Pl* (phyllosilicates, Cal)
13	26°08′93S	64°40′21W	Dike?	Intrudes fine-grained sandstone with lenses of gypsum	ANT22	Pl+Hbl+Ttn*+Pl+Kfs+Agt+Ap*
14	26°07′67S	64°40′71W	Dike?	Intrudes fine-grained sandstone with lenses of gypsum	ANT23	Hbl+Aug+Fe-Ti ox*+Pl+Kfs+Cpx+Ap*
1	26°08′25S	64°37′90W	WNW-striking dike	Isolated exposure	ANT24	Hbl+Aug+Fe-Ti ox *+Pl*

*Number of outcrop as referred in Figure 3.
†Main phenocryst, groundmass (in italics), and secondary (in brackets) minerals. Mineral abbreviations: Hbl—hornblende; Aug—augite; Pl—plagioclase; Cal—calcite; ox—oxides; Kfs—K-feldspar; Ol—olivine; Ap—apatite; Agt—aegirin-augite; Bt—biotite; Ttn—titanite; Cpx—clinopyroxene.

in the Arroyo Gonzalez, ~150 km to the north of the study area. This sequence includes the basal Metán Subgroup and the unconformably overlying Jujuy Subgroup (Gebhard et al., 1974; Galli and Hernández, 1999; Reynolds et al., 2000). The Metán Subgroup is formed, from base to top, by the Río Seco, Anta, and Jesús María Formations. In the study area, around the Cerro Colorado and Cerro Negro (Figs. 2 and 3), the Anta Formation directly overlies the Mealla Formation of the Salta Group. The Anta Formation is composed of well-stratified, reddish, fine-grained sandstone, siltstone, and mudstone interbedded with laminated greenish mudstone, whitish oolitic limestone, and abundant beds and lenses of gypsum. Geochronology analyses from tuffs collected on the Anta Formation have produced ages of 13.2–14.5 Ma (Reynolds et al., 2000). Lithofacies indicate that the Anta Formation corresponds to lacustrine and shallow-marine environments developed at the margins of the Miocene transgression of the Paraná Sea (Ramos and Aleman, 2000; Aceñolaza and Sprechmann, 2002; Vezzoli et al., 2009). The Jujuy Subgroup shows a basal unconformity and consists of the Guanaco and Piquete Formations. The Guanaco Formation is dominated by red and gray sandstones, siltstones, and conglomerates. Interbedded tuffs yielded U-Pb ages on zircon of 10.9 and 6.9 Ma (Viramonte et al., 1994b); the base of this unit is interpreted as younger than 9 Ma (Reynolds et al., 2000). The Guanaco Formation is in turn unconformably overlain by the Piquete Formation, which has an estimated age of 5–2 Ma (Reynolds et al., 2000) and is composed of dark-red polymictic cobble and boulder conglomerate, subordinate sandstone, and rare siltstone.

Volcanic and Structural Features

The Antilla volcanic rocks crop out in distinct lava bodies interpreted as lava flows and feeder dikes. Each exposure shows individual or superposed lavas with distinctive petrographic texture and composition (Table 1). On the northern side of the Cerro Negro, two dikes have N-S and NW-SE strike, respectively. They intruded a sedimentary sequence composed, from the base, of: (1) reddish and pinkish, laminated, fine-grained sandstone and siltstone interbedded with laminated greenish mudstone, and (2) stratified, whitish oolitic limestone, in 5–20-cm-thick beds. Lithofacies suggest the correlation of these sediments with the Anta Formation. On the southern side of the Cerro Negro (Río Quevitas), almost six different lava flows, 3–20 m thick, are interbedded within red and gray sandstone and laminated reddish and yellow siltstone. Several textures and structures at the lava-sediment interface suggest a synsedimentary emplacement of lava flows. The attribution of these sediments to a distinct Cenozoic lithostratigraphic unit is not obvious. Lithofacies may suggest a correlation with the Guanaco Formation. On the eastern side of the Cerro Negro, lavas are exposed as isolated relict hills representing WNW- to NW-striking dikes that are surrounded by yellowish and grayish, fine-grained sandstone and siltstone with lenses of gypsum that can be correlated to lithofacies of the Anta Formation.

The present regional structural setting of the Antilla area is represented by the N-S–striking Sierra de la Candelaria anticline, showing crystalline basement and Paleozoic rocks at its core (Fig. 3). On the eastern flank

of the fold, a N-S–striking and W-dipping high-angle fault thrusts the basement rocks over the Cenozoic sedimentary strata of the Orán Group, which generally gently (5°–1°) dip toward the east. In the footwall of this fault, the hill of the Cerro Negro is a small dome-shaped anticline plunging northward and southward and involving pink and red, medium-grained sandstones of the Pirgua Subgroup (Cretaceous Salta Group) at its core and the Cenozoic sediments of the Orán Group (Fig. 3). Due to the scarce erosion and abundant vegetation cover, no structures (fracture or fault) were observed throughout the studied area, except for a N-S–striking compressional dip-slip fault that was measured along the Río Quevitas on the southern side of the Cerro Negro. The fault plane dips 40° toward the east and offsets a lava flow (locality number 6 in Fig. 3 and Table 1) and the underlying Cenozoic sediments. All these deformations postdate the emplacement of the Antilla volcanics. Therefore, the only possible tectonic indicators of local or regional synvolcanic deformation are represented by the attitude of the Antilla dikes (Fig. 3), which coincides with the N-S– and NW-SE–trending directions of the regional structures.

Geochronology

Three samples of the Antilla lavas (Table 2) were selected for geochronological study (see analytical methods in Appendix) after macroscopic and petrographic inspections to exclude alteration. Sample ANT16 is a lava flow interbedded with red sandstone and siltstone along the Rio Quevitas, sample ANT24 represents a WNW-striking dike intruding the Anta Formation on the eastern side of the Cerro Negro, and sample ANT8 forms an isolated exposure near San Lorenzo (Table 1).

The K/Ar determinations are reported in Table 2. They give consistent ages of 4.83–4.67 Ma (Table 2). Viramonte et al. (2008) proposed an age of 7.7 Ma from Ar/Ar experiments on hornblende separates. This age is significantly older than the very precise and self-consistent K/Ar ones obtained in this work. Because of the lack of detailed data about the Ar/Ar experiments and of clear geological information about the Ar/Ar dated sample, it is not possible for us to comment on this age difference.

Petrography, Rock Classification, and Mineral Chemistry

The Antilla rocks have a SiO_2 content ranging from 49 to 61 wt%, LOI (loss on ignition)–free, and moderately high and variable alkali content (Table 3). The analyzed rocks fall in the alkaline field (Fig. 4), and in the K_2O versus Na_2O diagram, they plot in the field of the K-series (inset of Fig. 4). Most of the rocks are mildly nepheline-normative and range from trachybasalts to trachytes of the moderately alkaline series (Middlemost, 1980).

The Antilla rocks show a porphyritic texture, and the majority have high phenocryst content. The mafic samples are dominated by phenocrysts of calcic amphibole and clinopyroxene in variable mutual proportions (Table 1). The calcic amphibole has Mg# (molar Mg/Mg + Fe) ranging from 68 to 42 and commonly shows reverse zoning and disequilibrium rims. The clinopyroxene phenocrysts are represented by augite, with Mg# ranging from 88 to 67 and normal zoning (Table 4). Olivine is present as scarce, completely iddingsitized microcrystals. Apatite occurs as a common accessory. Labradorite plagioclase joins the phenocryst assemblage in part of the analyzed rocks (Table 1). The groundmass grain size is highly variable, from coarse in dikes to mainly medium-fine-grained in lava samples; it is composed of plagioclase, clinopyroxene, K-feldspar, Fe-Ti oxides, biotite, and olivine. The more silicic rocks (MgO < 3 wt%) contain phenocrysts of normally zoned plagioclase (andesine from $An_{49}Ab_{47}$ to $An_{26}Ab_{64}$, unzoned amphibole [Mg# around 50], aegirine-augite clinopyroxene [Mg# from 67 to 59 with rare Mg-rich cores], Na_2O up to 1.2 wt%; Table 4), large titanite and apatite crystals, Fe-Ti oxides, and minor biotite. The groundmass is made of the same minerals plus K-feldspar. Fe- and Cu-sulfides occur in some samples. Many rocks are altered to a variable extent, presenting phyllosilicates (probably chlorite minerals) substituting mafic grains in the groundmass, zeolites, and secondary calcite in the groundmass and filling vacuoles, sericitization on plagioclase, and, locally, albite and epidote.

Geochemistry

The chemical analyses of selected Antilla samples are presented in Table 3. The alkali content is rather variable, and two groups of samples, with lower and higher alkali content, may be recognized (Fig. 4). Some of the analyzed rocks (belonging mainly, but not exclusively, to the group with higher alkalies) show a relatively high value of LOI (Table 3). Although this high LOI value is related to a moderate alteration, we have preferred to report all the analyzed rocks because of the paucity of geochemical data on volcanic rocks related to the geologic context of the Antilla magmatic complex. Necessarily, we have taken into account the possible effects of the alteration process on the interpretation and discussion of the geochemical data, checking the eventuality of correlations between geochemical parameters and LOI.

The well-defined trends of the major elements, and in particular those of K_2O (very mobile element) and Al_2O_3, suggest that the

TABLE 2. UNSPIKED K-Ar AGES OF ANTILLA VOLCANIC ROCKS

Exp. no.	Split				Weighted mean	
	K (wt%, ±2σ)	Mass molten (g)	$^{40}Ar^*$ (%)	$^{40}Ar^*$ ($\times10^{-11}$ mol/g, ±1σ)	$^{40}Ar^*$ ($\times10^{-11}$ mol/g, ±1σ)	Age (Ma, ±2σ)
ANT-16						
7752	4.259 ± 0.043	0.49851	77.025	3.513	3.476 ± 0.012	4.70 ± 0.10
7773	4.259 ± 0.043	0.50398	34.197	3.440		
ANT-24						
7760	3.013 ± 0.030	1.07947	14.438	2.568	2.529 ± 0.009	4.83 ± 0.10
7786	3.013 ± 0.030	0.39333	10.253	2.490		
ANT-8						
7751	3.022 ± 0.030	0.42158	42.037	2.478	2.452 ± 0.009	4.67 ± 0.10
7789	3.022 ± 0.030	0.33998	35.567	2.428		

Note: Ages were calculated using the decay constants of Steiger and Jäger (1977).

TABLE 3. MAJOR- AND TRACE-ELEMENT ANALYSES OF REPRESENTATIVE SAMPLES OF ANTILLA VOLCANIC ROCKS

Sample	ANT 1	ANT 7	ANT 4	ANT 24	ANT 23	ANT 18	ANT 17	ANT 8	ANT 14	ANT 13	ANT 19	ANT 12	ANT 15	ANT 16	ANT 22
(wt%)															
SiO_2	47.27	46.69	50.71	50.07	47.21	49.83	45.96	53.43	49.2	49.85	51.01	49.11	49.99	58.48	55.80
TiO_2	1.25	1.36	1.12	1.11	1.21	1.18	1.15	0.92	0.88	0.86	0.89	0.98	0.89	0.54	0.58
Al_2O_3	13.73	13.89	15.85	15.71	15.28	15.71	16.03	17.11	17.65	17.89	17.93	17.07	17.9	17.67	18.66
Fe_2O_3tot.	9.13	9.57	8.76	8.51	11.00	10.54	10.58	7.67	7.82	7.69	7.56	8.37	7.74	4.56	4.57
MnO	0.14	0.16	0.16	0.16	0.20	0.16	0.21	0.16	0.17	0.20	0.30	0.21	0.17	0.14	0.17
MgO	7.99	7.32	6.34	5.81	5.61	4.98	4.89	3.61	2.56	2.53	2.34	2.29	2.18	1.53	1.03
CaO	10.35	12.21	8.71	8.28	8.64	6.58	7.23	7.64	6.03	5.52	8.15	6.92	6.34	4.36	4.78
Na_2O	2.81	2.69	2.95	3.62	4.43	4.35	4.52	3.79	5.71	6.33	3.82	5.03	5.83	4.57	5.76
K_2O	2.40	2.50	3.24	3.12	2.95	3.83	2.93	3.40	3.80	3.71	3.75	3.76	3.78	4.42	4.50
P_2O_5	0.25	0.28	0.31	0.31	0.62	0.56	0.67	0.35	0.44	0.42	0.48	0.52	0.46	0.20	0.19
LOI	4.23	4.36	1.95	2.25	3.62	2.28	4.77	1.34	3.56	4.96	2.99	4.76	4.45	2.63	1.81
Sum	99.55	100.10	101.03	99.42	99.02	99.96	97.82	99.73	99.10	98.94	100.00	99.22	97.85	100.77	98.95
Mg#	70	67	65	64	57	55	55	55	46	46	45	42	42	47	37
(ppm)															
Li	15.2	N.D.	23.5	N.D.	22.1	35	N.D.	18.9	60	N.D.	20.7	38	N.D.	34	24.8
Be	1.39	N.D.	1.90	N.D.	2.81	2.83	N.D.	2.44	4.7	N.D.	2.75	3.7	N.D.	4.5	5.1
Sc	43	N.D.	29	N.D.	23	25	N.D.	18	12	N.D.	10	15	N.D.	10	6
V	289	N.D.	241	N.D.	263	249	N.D.	180	178	N.D.	139	176	N.D.	78	89
Cr	157	N.D.	94	N.D.	95	32	N.D.	47	8	N.D.	3	10	N.D.	6	3
Co	38	N.D.	29	N.D.	32	29	N.D.	21	17	N.D.	14	19	N.D.	8	7
Ni	49	N.D.	28	N.D.	36	27	N.D.	15	9	N.D.	5	10	N.D.	4	5
Cu	98	N.D.	64	N.D.	88	82	N.D.	49	57	N.D.	15	53	N.D.	17	19
Rb	64	N.D.	92	N.D.	74	104	N.D.	112	106	N.D.	104	100	N.D.	162	162
Sr	707	N.D.	643	N.D.	886	679	N.D.	912	1025	N.D.	959	874	N.D.	770	1407
Y	19.7	N.D.	21.3	N.D.	28.0	29.2	N.D.	23.5	29.1	N.D.	27.3	34	N.D.	24.7	24.3
Zr	100	N.D.	130	N.D.	137	157	N.D.	170	201	N.D.	162	183	N.D.	216	261
Nb	18.6	N.D.	24.8	N.D.	27.0	23.9	N.D.	30.9	42	N.D.	24.2	41	N.D.	34	50
Cs	2.06	N.D.	2.14	N.D.	3.2	30.3	N.D.	0.91	9.2	N.D.	0.89	6.3	N.D.	3.5	8.1
Ba	480	N.D.	677	N.D.	502	733	N.D.	765	629	N.D.	601	529	N.D.	544	729
La	17.7	N.D.	23.7	N.D.	29.6	31.0	N.D.	30.9	42	N.D.	30.6	42	N.D.	38	49
Ce	36	N.D.	46	N.D.	61	63	N.D.	59	79	N.D.	61	83	N.D.	68	88
Pr	4.7	N.D.	5.6	N.D.	7.7	7.9	N.D.	6.8	9.3	N.D.	7.7	10.4	N.D.	7.7	9.7
Nd	20.3	N.D.	23.1	N.D.	32.2	33.0	N.D.	26.3	38	N.D.	32.2	41	N.D.	28.2	35
Sm	4.6	N.D.	4.8	N.D.	7.1	7.1	N.D.	5.2	7.5	N.D.	6.6	8.5	N.D.	5.3	6.1
Eu	1.36	N.D.	1.43	N.D.	2.13	1.99	N.D.	1.51	2.16	N.D.	1.95	2.48	N.D.	1.47	1.81
Gd	3.8	N.D.	4.3	N.D.	5.9	5.8	N.D.	4.6	6.1	N.D.	5.8	6.8	N.D.	4.7	4.8
Tb	0.59	N.D.	0.67	N.D.	0.91	0.91	N.D.	0.70	0.89	N.D.	0.87	1.07	N.D.	0.71	0.69
Dy	3.5	N.D.	3.8	N.D.	5.1	5.2	N.D.	4.0	5.1	N.D.	4.9	5.9	N.D.	4.1	4.0
Ho	0.73	N.D.	0.79	N.D.	1.02	1.09	N.D.	0.79	1.01	N.D.	1.00	1.21	N.D.	0.82	0.83
Er	1.85	N.D.	2.05	N.D.	2.56	2.75	N.D.	2.16	2.65	N.D.	2.56	3.09	N.D.	2.30	2.16
Tm	0.26	N.D.	0.31	N.D.	0.36	0.38	N.D.	0.32	0.39	N.D.	0.37	0.46	N.D.	0.36	0.35
Yb	1.73	N.D.	1.87	N.D.	2.29	2.54	N.D.	2.01	2.61	N.D.	2.36	2.82	N.D.	2.35	2.28
Lu	0.23	N.D.	0.29	N.D.	0.34	0.35	N.D.	0.32	0.36	N.D.	0.35	0.39	N.D.	0.36	0.34
Hf	2.67	N.D.	3.33	N.D.	3.5	4.2	N.D.	4.1	4.6	N.D.	4.2	4.4	N.D.	4.9	5.6
Ta	1.10	N.D.	1.42	N.D.	1.67	1.40	N.D.	1.76	2.35	N.D.	1.52	2.50	N.D.	2.06	2.83
Tl	0.35	N.D.	0.41	N.D.	0.52	0.49	N.D.	0.52	0.79	N.D.	0.52	0.75	N.D.	1.08	1.41
Pb	7.1	N.D.	8.6	N.D.	10.8	11.6	N.D.	10.7	29.7	N.D.	13.7	14.0	N.D.	14.3	17.7
Th	3.7	N.D.	5.3	N.D.	4.8	6.8	N.D.	7.1	9.3	N.D.	6.4	7.3	N.D.	10.2	11.6
U	1.33	N.D.	1.9	N.D.	1.77	2	N.D.	2.45	3.6	N.D.	2.62	2.72	N.D.	4.1	4
La/Ta	16	N.D.	17	N.D.	18	22	N.D.	18	18	N.D.	20	17	N.D.	18	17
Zr/Y	5	N.D.	6	N.D.	5	5	N.D.	7	7	N.D.	6	5	N.D.	9	11

Note: Whole-rock X-ray fluorescence (XRF) analyses of major oxides were done on fused samples with an ARL 9400 XPp instrument at the Dipartimento di Scienze della Terra, University of Pisa, Italy. Accuracy is 4–7% for concentrations <1 wt%, 2–4% for concentrations 1–10 wt%, 1% for concentrations >10 wt%. Trace-element analyses were carried out on a selection of samples with an inductively coupled plasma–mass spectrometer (ICP-MS; VG PQII Plus) at Dipartimento di Scienze della Terra, University of Pisa, Italy, with accuracy to within ±5%. LOI—loss on ignition; N.D.—Not determined.

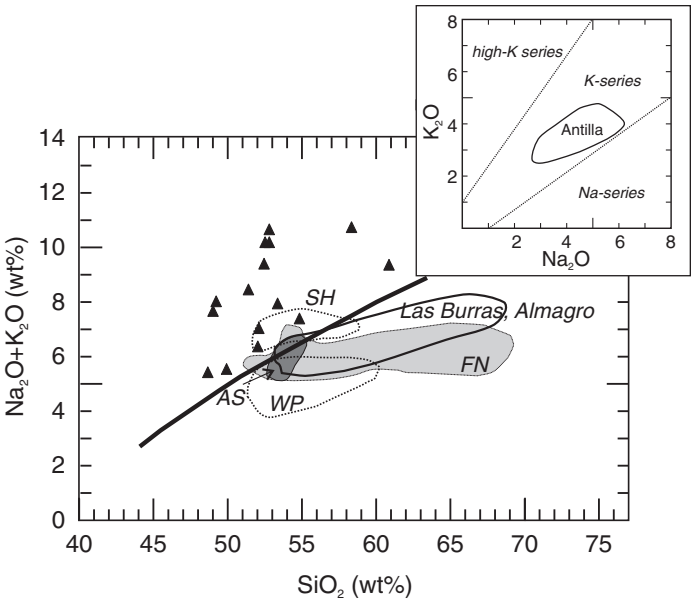

Figure 4. Diagram of K_2O + Na_2O versus SiO_2 for the Antilla (full triangles) rocks, plotted along with the main volcanic and intrusive complexes in the backarc region between 24°S and 27°S. Black line divides the alkaline and subalkaline fields (Irvine and Baragar, 1981). Las Burras and Almagro—Mazzuoli et al. (2008); SH—Puna Pliocene–Quaternary shoshonite rocks (Kay et al., 1994); WP—Puna Pliocene–Quaternary intraplate rocks (Kay et al., 1994); AS—Antofagasta de La Sierra (Galan satellite mafic rocks; Francis et al., 1989; Kraemer et al., 1999); FN—Farallón Negro (Halter et al., 2004).

alteration processes did not deeply modify the content of these elements (Fig. 5). When plotted with MgO taken as a differentiation index, alkali and Al_2O_3 increase regularly with decreasing MgO, whereas TiO_2, FeO, and CaO exhibit a negative trend (Fig. 5), indicating fractionation of mafic minerals such as those in the phenocrysts assemblage of the mafic and intermediate rocks, i.e., clinopyroxene, amphibole, and titanite. Regarding the trace elements, the Antilla samples describe regular and well-defined trends in variation diagrams of all the compatible or the incompatible elements (Fig. 5). The two groups observed in the alkali-silica diagram are evident in Na_2O, Fe_2O_3, and P_2O_5 variation diagrams, but are not particularly highlighted by the trace element (Fig. 5), except for a very moderate dispersion of Zr and Th contents in the mafic analyzed samples (Table 3).

In the spider diagrams of trace elements normalized to the primitive mantle (Fig. 6A), the Antilla mafic samples display positive anomalies of Rb, Th, K, and Pb and moderate negative troughs of Nb, Ta, and Ti. The rare earth element (REE) patterns of the mafic Antilla samples are moderately fractionated and show no Eu anomaly (Fig. 6B). Also, the most differentiated samples, which bear plagioclase as main phenocrysts, do not show Eu anomalies, indicating that crystallization occurred at high-oxygen-fugacity conditions. This evidence, joined to the petrographic features suggesting a large presence of hydrous minerals, may be taken as an indication of the volatile-rich nature of Antilla magmas.

The Antilla samples show Sr isotopic ratios ranging from 0.704360 to 0.706406 and Nd from 0.512764 to 0.512625 (Table 5; Fig. 7). In the $^{87}Sr/^{86}Sr$ versus $^{143}Nd/^{144}Nd$ diagram, the Sr and Nd isotopic ratios of Antilla rocks are correlated to each other, following the Sr and Nd Central Andes main trend, but neither the Sr nor the Nd ratio shows any correlation with the degree of evolution represented by SiO_2.

TABLE 4. REPRESENTATIVE ANALYSES OF THE MAIN MINERALS IN ANTILLA VOLCANIC ROCKS

Clinopyroxene

	ANT23		ANT4		ANT22		ANT12	
	Core	Rim	Core	Rim	Core	Rim	Core	Rim
SiO_2	52.47	47.00	49.26	50.49	50.94	46.85	45.75	46.96
TiO_2	0.45	1.32	0.83	0.81	0.63	1.25	1.40	0.75
Al_2O_3	2.75	6.97	5.44	3.35	3.03	6.61	7.84	5.36
FeO	4.03	9.09	8.29	8.40	6.70	10.37	10.10	14.10
MnO	b.d.l.*	0.23	0.26	0.35	b.d.l.*	0.41	0.58	1.09
MgO	16.41	12.04	12.74	14.12	14.76	10.59	10.62	8.50
CaO	23.80	22.90	22.72	22.16	23.38	23.29	23.12	22.04
Na_2O	0.09	0.45	0.44	0.31	0.56	0.62	0.59	1.20
Wo	47.81	48.98	48.42	45.82	47.57	50.15	50.00	48.19
En	45.87	35.84	37.79	40.63	41.79	31.73	31.96	25.86
Fs	6.32	15.18	13.79	13.56	10.64	18.12	18.04	25.95
Mg#	87.9	70.2	73.3	75.0	79.7	64.5	68.4	54.5

Amphibole

	ANT23		ANT4		ANT22		ANT12	
	Core	Rim	Core	Rim	Core	Rim	Core	Rim
SiO_2	39.08	41.49	41.62	41.51	40.14	40.42	39.87	39.51
TiO_2	2.70	2.66	2.36	2.33	2.79	2.58	2.51	3.21
Al_2O_3	15.15	13.81	14.55	14.57	12.77	13.35	15.03	13.60
FeO	17.89	13.56	11.58	12.11	18.56	16.39	14.66	17.81
MnO	0.39	0.25	0.16	0.20	0.88	0.48	0.31	0.56
MgO	9.26	12.63	13.84	13.40	9.06	10.71	11.41	9.25
CaO	11.81	12.01	12.26	12.29	11.65	12.03	12.32	11.85
Na_2O	2.05	2.00	1.79	1.99	2.36	2.46	2.50	2.41
K_2O	1.67	1.58	1.83	1.61	1.78	1.59	1.38	1.80
Mg#	48.0	62.4	68.0	66.4	46.5	53.8	58.1	48.1

Feldspar

	ANT23		ANT23		ANT22		ANT12	
	Core	Rim	Gm†	Gm	Core	Rim	Core	Rim
SiO_2	44.51	45.24	44.34	64.06	55.29	58.54	58.86	61.16
Al_2O_3	35.57	34.91	35.67	20.54	28.43	26.28	26.06	24.07
FeO	b.d.l.*	0.13	b.d.l.*	0.31	0.34	0.37	0.45	0.53
CaO	15.14	14.95	15.09	1.11	10.02	7.57	7.20	5.32
Na_2O	4.72	4.65	4.85	4.38	5.35	6.39	6.48	7.28
K_2O	0.06	0.12	0.06	9.61	0.57	0.85	0.94	1.64
An	63.74	63.60	63.04	5.42	49.17	37.58	35.92	26.02
Ab	35.96	35.80	36.66	38.70	47.50	57.40	58.50	64.43
Or	0.30	0.61	0.30	55.87	3.33	5.02	5.58	9.55

Note: Analyses were performed on polished rock sections of samples ANT4, 18, 23 (whole-rock MgO > 3 wt%) and ANT12 and 22 (whole-rock MgO < 3 wt%), with a Philips XL30 scanning electron microscope equipped with microanalysis EDAX (standard-less software DXi4) at Dipartimento di Scienze della Terra, University of Pisa, Italy (acceleration voltage 20 kV, beam current 5 nA, live time 100 s). The accuracy is better than 0.5% if abundance is >15 wt%, 1% if abundance is around 5 wt%, and better than 20% if abundance is around 0.5 wt%.

*Below detection limit.

† Groundmass.

DISCUSSION

Magma Source Characteristics

The Antilla volcanics are moderately alkaline and involve mafic rocks with a Mg-value around 70 and a maximum Cr and Ni content of 147 and 49 ppm, respectively. Moderately differentiated rocks with SiO_2 content close to 60 wt% (Table 3) are present as well. The scarcity of olivine, the moderate Ni and Cr content, and the chemical composition of phenocrysts

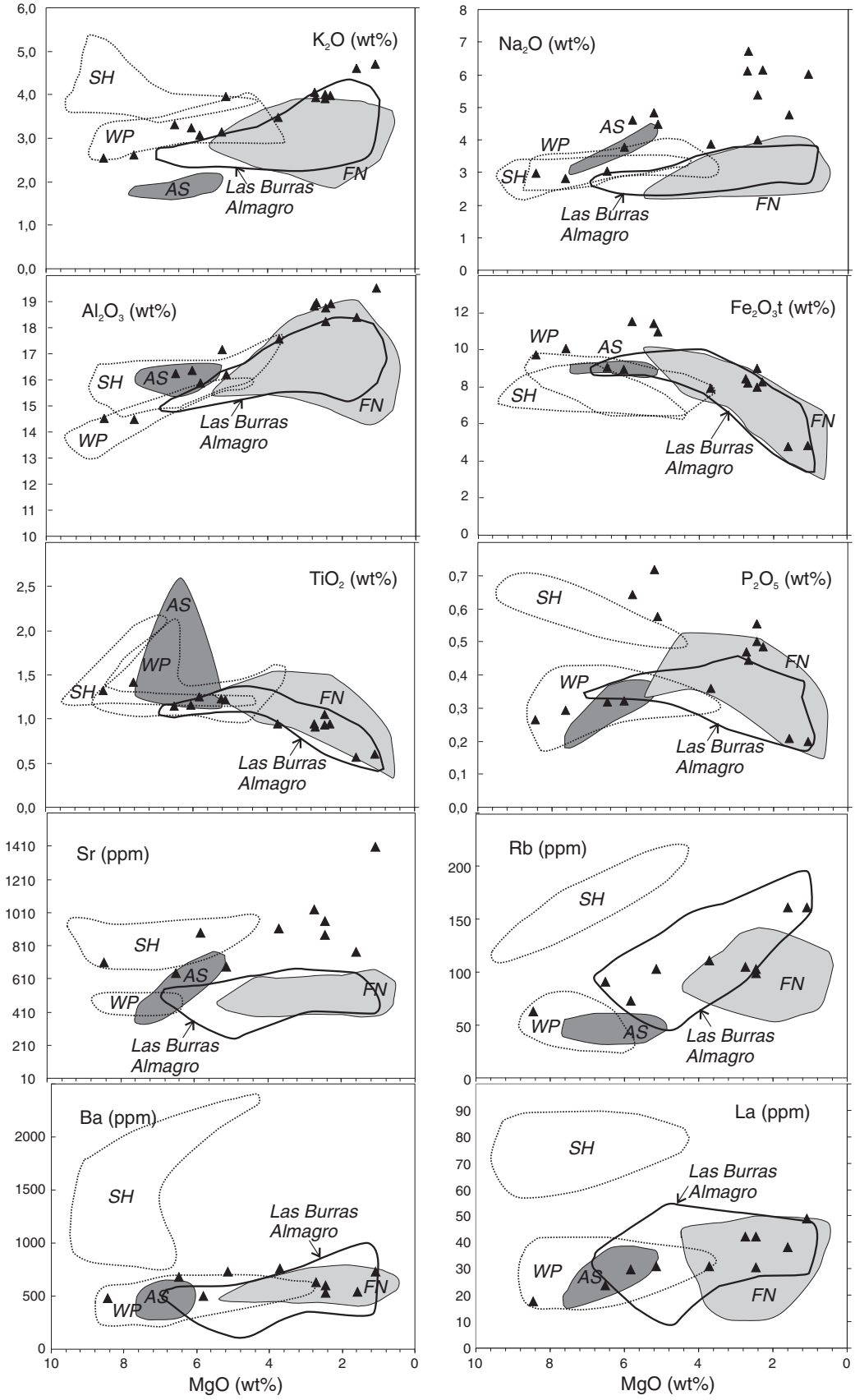

Figure 5. Variation diagrams of selected major and trace elements showing Antilla rocks compared to the backarc volcanic products between 24°S and 27°S. Symbols and labels of fields are as in Figure 4.

L81 2nd pages / 12 of 19

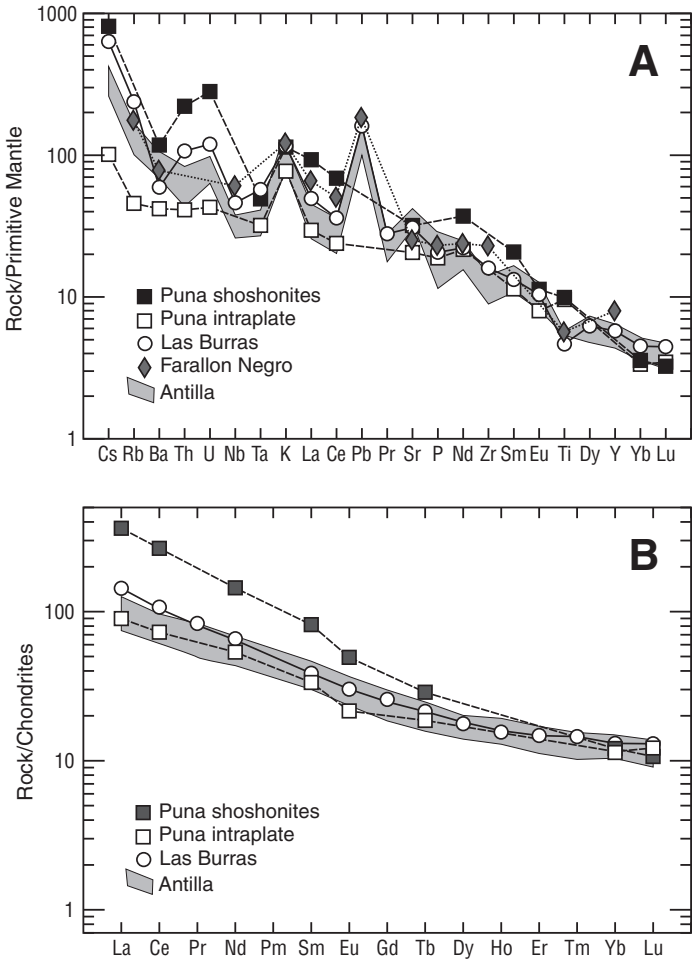

Figure 6. (A) Primitive mantle–normalized spider diagrams (normalization factors from McDonough and Sun, 1995) of Antilla mafic rocks, compared to the backarc mafic volcanic products between 24°S and 27°S. (B) Chondrite-normalized rare earth element (REE) patterns (normalization factors from McDonough and Sun, 1995) of Antilla mafic rocks, compared to the backarc mafic volcanic products between 24°S and 27°S.

TABLE 5. WHOLE-ROCK Sr AND Nd ISOTOPIC MEASUREMENTS OF ANTILLA ROCKS

Sample ID	$^{87}Sr/^{86}Sr$	Standard deviation	Runs	$^{143}Nd/^{144}Nd$	Standard deviation	Runs
ANT1	0.704345	0.000003	97/100	0.512737	0.000003	95/100
				0.512741	0.000004	96/100
ANT4	0.704372	0.000003	93/100	0.512738	0.000005	94/100
				0.512724	0.000003	94/100
ANT8	0.704361	0.000004	94/100	0.512702	0.000003	97/100
	0.704360	0.000004	94/100			
ANT12	0.704744	0.000003	97/100	0.512750	0.000003	96/100
ANT14	0.704592	0.000004	94/100	0.512765	0.000008	92/100
ANT16	0.705158	0.000003	93/100	0.512660	0.000004	96/100
ANT18	0.706406	0.000004	95/100	0.512625	0.000004	93/100
	0.706396	0.000004	96/100			
ANT19	0.704756	0.000004	96/100	0.512701	0.000005	97/100
ANT22	0.704236	0.000004	98/100	0.512781	0.000006	94/100
ANT23	0.704428	0.000004	95/100	0.512764	0.000004	95/100

Note: Analyses were performed at the IUEM (European Institute for Marine Studies, Brest, France). Samples were dissolved with a mixture of HF–HNO_3 for 48 h at 95 °C, and then dried at the same temperature until the complete evaporation of acids. Dry samples were dissolved again with HCl acid prior to the elution. Chemical separation for Sr and rare earth elements (REEs) was performed on cationic DOWEX® AG50X8 columns. Sr part was kept and processed another time in the same column to efficiently separate Sr from Rb and Ca. Nd was further eluted on LnSpec Eichrom resin. Isotopic measurements were performed on a Thermo Electron™ Triton T1. Sr was run on a single W filament with Ta activator, while Nd was run on a Re double filament. The NBS 987 (for Sr) and La Jolla (for Nd) standards were run regularly to check the measurements: average value $^{87}Sr/^{86}Sr = 0.710266$ ($n = 5$); average value $^{143}Nd/^{144}Nd = 0.511847$ ($n = 7$). Blanks were less than 160 pg for Sr and 150 pg for Nd, and therefore were considered negligible relative to the concentrations for these elements in the samples.

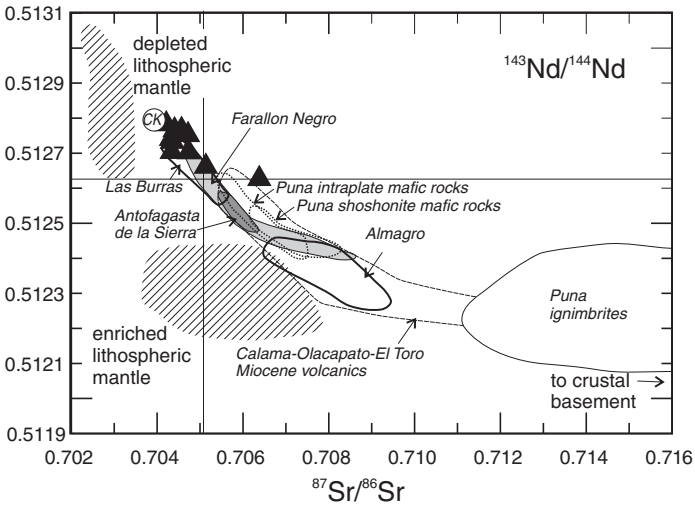

Figure 7. Diagram of $^{143}Nd/^{144}Nd$ versus $^{87}Sr/^{86}Sr$ for Antilla rocks compared to the backarc volcanic products between 24°S and 27°S. Symbols and labels of fields are as in Figure 4. Dashed mantle fields from Lucassen et al. (2002, 2005). CK—Chiar Kkollou basalt, Davidson and de Silva (1995).

(Tables 3 and 4) suggest that even the most primitive rocks underwent some differentiation processes.

The low values of discriminant trace-element ratios such as La/Ta and Zr/Y indicate an intraplate character (Fig. 6A). The low Ba/Nb ratio excludes a contribution from subduction-related fluids during the partial melting of the mantle source (Fig. 8).

Compared to the backarc mafic Miocene to Quaternary products between 24°S and 27°S, the Antilla samples show some trace-element characteristics similar to intraplate mafic rocks (i.e., Las Burras, Farallón Negro, and Puna monogenetic centers) in the positive anomalies of Rb and K and the negative anomaly of Ti (Fig. 6A), the moderately fractionated REE patterns (Fig. 6B), and the weak heavy (H) REE depletion. The latter suggests the absence of residual garnet in the mantle source and a melt equilibration shallower than 60–70 km (Fig. 9). However, the Antilla mafic rocks differ from the Puna intraplate rocks, even the most primitive basalt yet reported by Drew et al. (2009), for their alkaline nature, the lower content of silica, Cr, and Ni with a comparable MgO content, and the lower Sr and higher Nd isotope ratios. The high porphyricity and the abundance of volatile-bearing minerals are comparable to the rocks emplaced at the eastern margins of the backarc region (i.e., Farallón Negro, Las Burras, and Almagro). The remarkably primitive Sr and Nd isotope ratios of Antilla rocks plot not far from the 20 Ma Chiar Kkollu basalt (Fig. 7), which is considered to be a near-primary intraplate magma in the Central Andes (Davidson and de Silva, 1995). Moreover, the Antilla rocks overlap the composition of Las Burras, the most primitive rocks along the Calama–Olacapato–El Toro transversal structure at 24°S (Mazzuoli et al.,

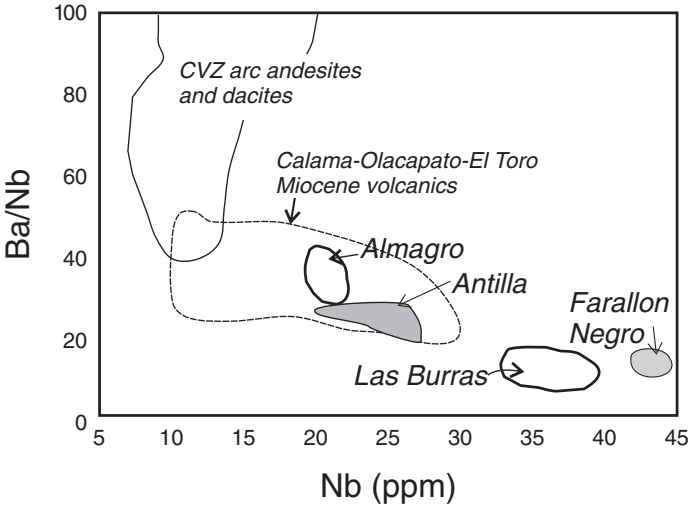

Figure 8. Ba/Nb versus Nb trace-element diagram for the Antilla mafic rocks compared to the backarc mafic volcanic products between 24°S and 27°S. Field for the Central volcanic zone (CVZ) arc rocks is also reported (Trumbull et al., 1999).

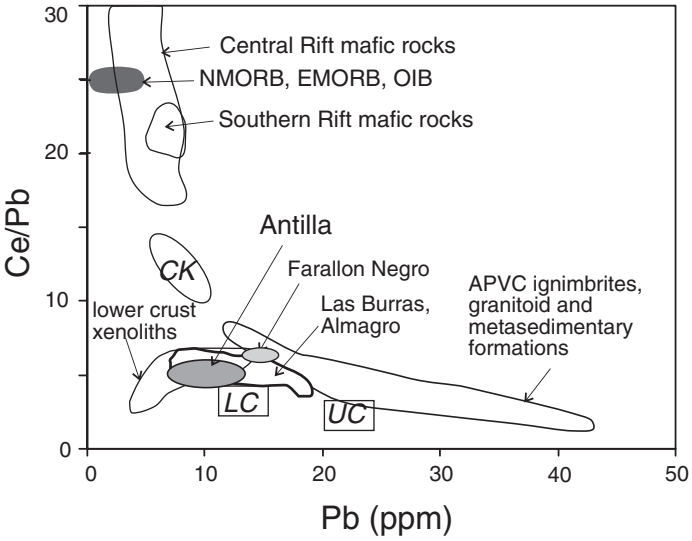

Figure 9. Ce/Pb versus Pb trace-element diagram for the mafic Antilla rocks compared to the backarc volcanic products between 24°S and 27°S. Puna crustal ignimbrites are from Francis et al. (1989) and Siebel et al. (2001). LC—lower crust; UC—upper crust; CK—Chiar Kkollou basalt, Davidson and de Silva (1995); APVC—Altiplano-Puna volcanic complex, de Silva (1989); NMORB-normal-mid-ocean ridge basalt; EMORB-enriched-mid-ocean ridge basalt; OIB-ocean-island basalt.

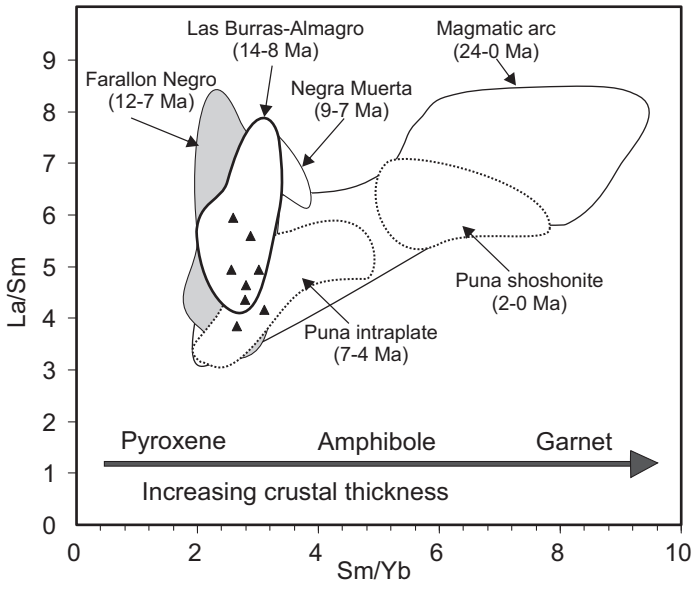

Figure 10. La/Sm versus Sm/Yb ratios for southern Puna Plateau backarc and magmatic arc rocks (23–28°S). Data sources are as in Figures 4 and 8.

2008), and approach the composition of the Mesozoic peridotite xenoliths reported by Lucassen et al. (2002, 2005).

Because of the Sr and Nd isotopic compositions, the moderately alkaline character, and the shallow depth of the source, we interpreted that Antilla primitive magmas originated by partial melting of the depleted subcontinental mantle. The variable alkali enrichment of these mafic rocks, uncorrelated with the isotopic composition, may suggest variable degrees of partial melting.

The differentiation of the Antilla products was dominated by fractional crystallization processes. The isotopic composition is not correlated with differentiation, indicating a minor role for assimilation of crustal material. The Antilla volcanics have a low Ce/Pb ratio and a low Pb content (Fig. 10), similar to the Farallón Negro and Las Burras–Almagro rocks, close to the field representing the lower-crust xenoliths of Lucassen et al. (1999). Therefore, a minor involvement of lower crust, characterized by low Ce/Pb ratios and low Sr and high Nd isotopic ratios, may have had a role in determining the small range of isotopic composition shown by the mafic Antilla magmas (Fig. 7).

Antilla Volcanism in the Frame of the Evolution of the Southern Central Andes

In the backarc sector of the southern Central Andes, between 24°S and 27°S, volcanic rocks with distinct affinities have been erupting since the middle Miocene (Fig. 11A). When considering the most primitive of these rocks, three main groups can be distinguished: (1) high-K calc-alkaline rocks, associated with Miocene stratovolcanoes and monogenetic centers, mainly located in the northern (e.g., Negra Muerta) and southern (e.g., Pasto Ventura) parts of the region; (2) shoshonitic rocks, erupted in the past 2 Ma by small monogenetic centers clustered in the northeastern part of the region (i.e., San Geronimo and Chorrillos); and (3) products with intraplate affinity (low La/Ta and Zr/Y), erupted since Miocene times up to Quaternary times by monogenetic centers, emplaced in a large part of the Puna, and by lava domes and intrusions in the Eastern Cordillera and Santa Barbara System (i.e., Las Burras, Almagro, Tuzgle, and Farallón Negro).

The geochemical features of the Antilla mafic lavas relate these rocks to the mafic intraplate volcanism at the margin of the backarc region, and suggest that these primitive magmas originated by partial melting of the depleted subcontinental mantle.

A question arises: why did the mantle undergo melting so far from the active volcanic arc? The lack of a subduction imprint in the Antilla rocks and the depth of the slab beneath Antilla exclude mantle melting due to subduction-derived fluids or melts. Other scenarios must be examined that take into account the geodynamic setting of Antilla. The generation of mantle-derived magmas in an intraplate setting may occur in an

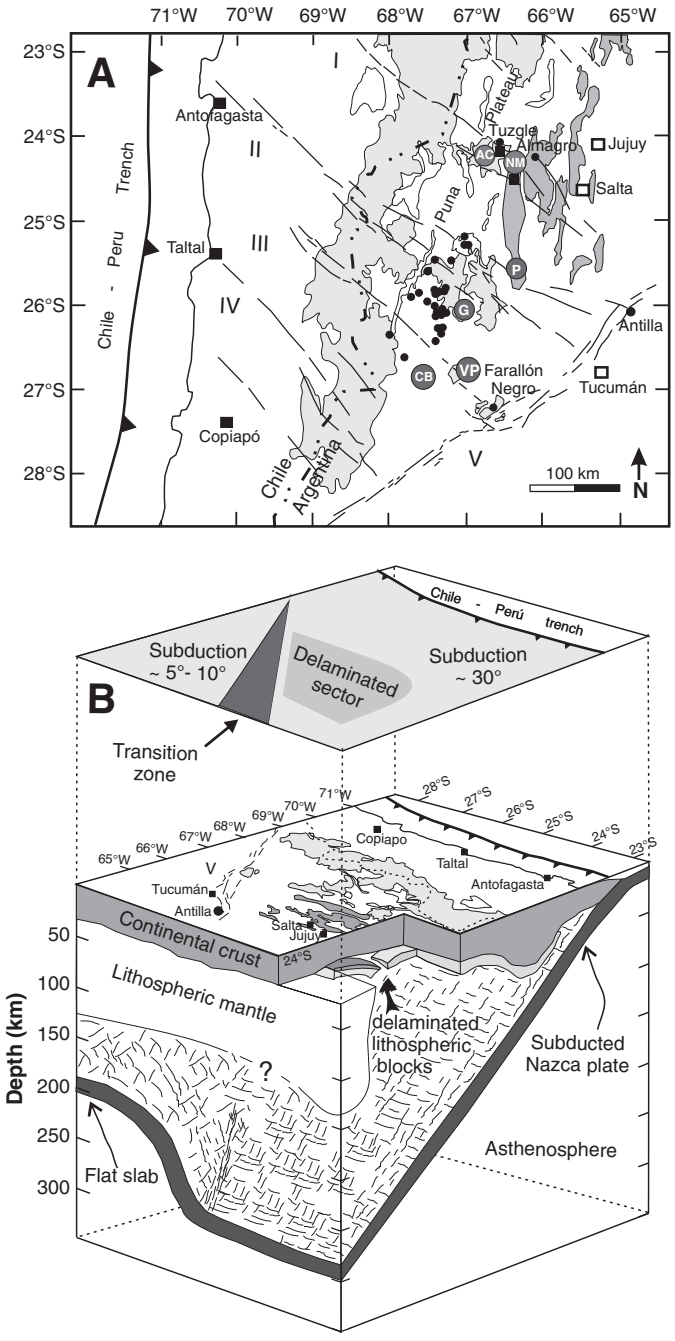

Figure 11. (A) Geologic sketch map showing the Miocene to present-day backarc intraplate volcanism (solid circles), shoshonite centers (black squares), and the major ignimbrite-related calderas of the backarc region between 24°S and 27°S. Data sources: Coira et al. (1993); Coira and Kay (1993); Kay et al. (1994); Schnurr et al. (2007); Harris et al. (2004); Risse et al. (2008); Mazzuoli et al. (2008). Caldera names: AC—Aguas Calientes (14–7 Ma); CB—Cerro Blanco (0–3 Ma); G—Galán; NM—Negra Muerta (6–9 Ma); P—Pucarillas; VP—Vicuña Pampa; compiled from Trumbull et al. (2006); Riller et al. (2001); Petrinovic et al. (2005); Guzmán (2009). Tectonic lineaments: I—Calama–Olacapato–El Toro, II—Archibarca, III—Culampaja, IV—Ojos del Salado, V—Tucumán transfer zone; compiled from Mon (1979); Salfity (1985); Chernicoff et al. (2002); de Urreztieta et al. (1996). (B) Three-dimensional conceptual cartoon of the southern Central Andes (23°S–28°S), showing the Nazca plate subduction with the transition from 30° of dip to a flat setting, and the delamination sector connected to intraplate magmatism in the southern Puna Plateau.

extensional regime, producing large magma volumes, but both these conditions are lacking at Antilla. On the other hand, geophysical data at 25°S indicate a relatively thin lithosphere (Asch et al., 2006), which has been related to the occurrence of processes of foundering of the lower portions of the lithosphere itself, invoked in the southern Puna Plateau since the middle Miocene (Fig. 11B; Kay et al., 1994; Asch et al., 2006; Mazzuoli et al., 2008; Kay and Coira, 2009). These processes were a consequence of crustal thickening and shortening during the main Andean compressional tectonic phase (Kay and Coira, 2009). Replacement of portions of the lower lithosphere by hot asthenosphere has been interpreted as the cause of the mantle melting responsible for the Pliocene pulse of mafic magmas in the Puna, suggesting a spatial correlation between their intraplate-like geochemical signature and location of lithospheric foundering beneath the plateau (Kay et al., 1994). The new thermal regime due to the rise of asthenosphere led to the partial melting of the continental crust (de Silva et al., 2006), too, originating the large volumes of felsic magmas erupted in this Andean sector (i.e., Cerro Galan; Fig. 11B). Antilla is the easternmost volcano with intraplate-like signature, east of the Galan area, and is coeval with the acme of Pliocene magmatism in the Puna. Therefore, we favor the hypothesis that the generation of Antilla primary magmas was related to a scenario of foundering of limited portions of the lower lithosphere, inducing asthenospheric upflow and consequent melting of lower portions of the subcontinental mantle.

The results of the study of the Antilla volcanic complex enable us to provide insights into the lithospheric mantle composition in the Andean foreland. The Antilla rocks, which have low Sr and high Nd isotopic ratios, and which were emplaced out of the zone where the crust was largely affected by partial melting, represent the least contaminated products of the Central Andes backarc magmatism during the Pliocene. The comparison of the petrological characteristics of Antilla with those of the most primitive magmas of monogenetic mafic centers of the Puna Plateau indicate that, whereas under the Puna part of the mafic magmatism requires the presence of an aged, metasomatized, subcontinental lithospheric mantle portion (Drew et al., 2009), in the eastern backarc the subcontinental mantle has a depleted isotopic composition. Similar indications have been found at 24°S in the Las Burras older rocks (Mazzuoli et al., 2008).

At the margin of the backarc region, the crust did not obliterate the mantle imprint of magmas, and isotopically primitive compositions were repeatedly erupted (Figs. 11A and 12). As a whole, the mafic volcanic products emitted from the middle Miocene to Quaternary at the margins of the backarc region (Fig. 11A) show variable geochemical features, i.e., Farallón Negro, Almagro, and the Puna shoshonitic volcanism show higher Ba/Nb and La/Ta, and Almagro mafic lavas show notably higher Sr and lower Nd isotopic ratios than Antilla (Fig. 12). This picture suggests that these magmas were derived from a lithospheric mantle containing regions modified by inputs of subduction-related metasomatizing fluids that underwent different degrees of partial melting in the frame of the lithospheric delamination process.

Eastward, beyond these magmatic complexes, Miocene-Quaternary backarc volcanic activity was apparently absent (Fig. 1). The distribution and timing of the backarc magmas have some important structural implications. The absence of magmatic centers east of Antilla in the Andean foreland may be explained by the presence of pure compressive structures that inhibited the ascent of magma despite the possible presence of partially molten rocks at depth, as was proposed for the eastern termination of the magmatic belt along the Calama–Olacapato–El Toro (Acocella et al., 2007). The inferred extension of the western edge of the Brazilian craton beneath the Andes to ~65°–66°W at the latitude of 18°–24°S (Beck and Zandt, 2002; Babeyko and Sobolev, 2005) coincides with volcanism termination along the Calama–Olacapato–El Toro lineament (Mazzuoli et

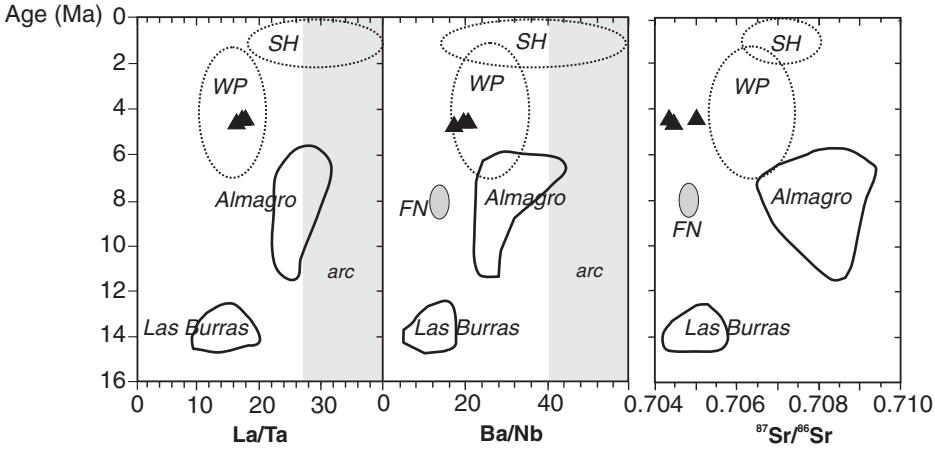

Figure 12. Age versus discriminating ratios La/Ta and Ba/Nb and the Sr isotopic ratio for the Antilla samples (black triangles). SH—Puna shoshonites (Kay et al., 1994); WP—Puna intraplate mafic rocks (Kay et al., 1994); FN—Farallón Negro (Halter et al., 2004); Las Burras and Almagro (Mazzuoli et al., 2008).

al., 2008) and may be considered as a concurrent cause of backarc volcanism absence east of 64°W also along the southern lineaments.

The age of the Antilla lavas corresponds to the acme of mafic and ignimbrite volcanic activity around 25°S (Risse et al., 2008). The diagram in Figure 13 shows the relationships between the ages and latitude of the backarc magmatic centers in the interval between 24°S and 27°S. This diagram can give some general indications, despite being limited by either incomplete sampling or the lack of age determinations. At around 24°S, in coincidence with an ~150 km segment of the Calama–Olacapato–El Toro lineament, volcanic activity lasted from ca. 14 Ma until 6 Ma and then became scarce and dominated by monogenetic centers (Kay et al., 1994). Furthermore, volcanism concentrates in a narrow belt around 24°S. Southward, between 25°S and 26°S, volcanism started at ca. 7.3 Ma and had an acme at 4–5 Ma (Risse et al., 2008); the activity, which is recorded by many age data, was widespread in a wider latitude interval than the Calama–Olacapato–El Toro belt. In this area, the NNE-SSW–striking faults, parallel to the trend of Antofalla salar (Marrett and Strecker, 2000) and Tucumán transfer zone, could have played an important role in magma ascent (Risse et al., 2008). South of 26.5°S, the only age determinations are related to the long-lived volcano Farallón Negro, aligned with Antilla along the important Tucumán lineament.

The time distribution of the backarc magmatism, and in particular, the onset of the mafic intraplate backarc volcanism, which is related to the delamination process, can be read in the frame of the tectonic history of this sector of the Central Andes. Two distinct tectonic phases have been recognized: an older NW-SE compressional event that produced thrust faults since ca. 10 Ma, and a younger NE-SW or E-W shortening event with a component of N-S extension that reactivated previous thrust faults and transverse lineaments with extensional and strike-slip components from the Pliocene to the Quaternary (5–2 Ma) (Allmendinger, 1986; Allmendinger et al., 1989; Cladouhos et al., 1994; Marrett et al., 1994; Marrett and Strecker, 2000). The ages of the oldest volcanoes with intraplate affinity at 7 Ma could record, as suggested by some authors (Kay et al., 1999; Kraemer et al., 1999; Risse et al., 2008), the beginning of the change in regional stress conditions in the southern Puna Plateau (Marrett and Emerman, 1992), and the ages of 5.3–3.6 Ma could represent the acme of volcanic activity linked to the change in stress regime. This process is recorded by the volcanic activity at 25–26°S, whereas at ~24°S, a compressional regime was predominant due to the underthrusting of the Brazilian Shield under the Andes structure (Acocella et al., 2007; Mazzuoli et al., 2008), partially preventing the storage and ascent of magmas.

In this frame, the Antilla volcanic complex takes on a particular interest because it defines the southeastern limit of the magmatic effects of the lithospheric delamination process and of the thinned lithosphere. Furthermore, its geological position at the intersection between the Archibarca-Galan fault system and the Tucumán transfer zone could suggest that the

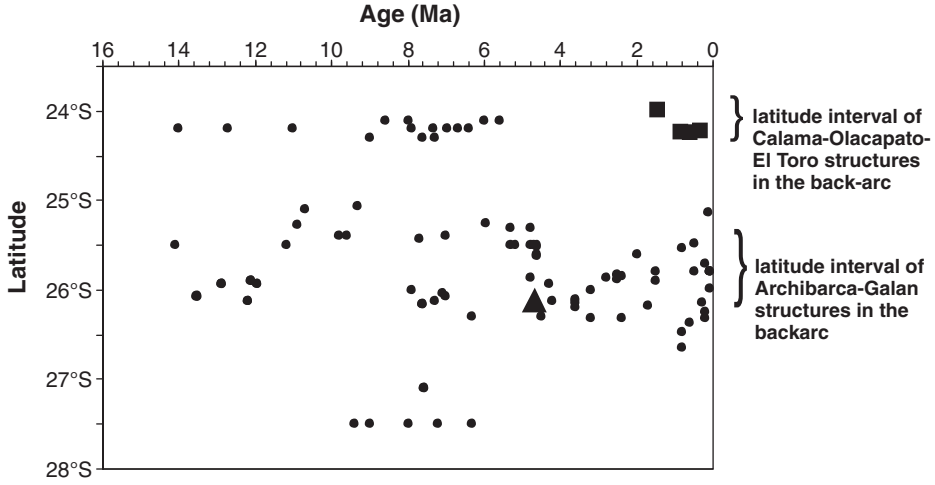

Figure 13. Age of backarc volcanism versus latitude between 24°S and 27°S. Black triangle—Antilla; dots—backarc monogenetic mafic centers, stratovolcanoes, and caldera complexes; black squares—shoshonitic centers. Data are from this work; Kraemer et al. (1999); Halter et al. (2004); Petrinovic et al. (2005); Guzman et al. (2006); Risse et al. (2008), and references therein; Mazzuoli et al. (2008); and Guzmán (2009).

latter lineament, practically matching the dipping direction of the southward shallowing of the subducting Nazca plate (Fig. 12), played an important role in the ascent of magmas (i.e., Farallón Negro, Portezuelo de las Ánimas, and Antilla), extending backarc magmatism to 64°W.

CONCLUSIONS

The study of the Pliocene Antilla rocks, the easternmost magmatic outcrops in the Central Andes between 24°S and 27°S, was the starting point for a revision of our understanding of the backarc volcanism in this sector. The Antilla rocks are prevalently mafic, and have geochemical characteristics similar to those of mafic intraplate volcanism in the backarc, and their Sr and Nd isotopic characteristics are among the most primitive recorded in the backarc lavas. The Antilla rocks, with an age of 4.7 Ma, were emplaced coeval with the acme of activity of the mafic monogenetic intraplate centers and the felsic volcanoes erupting crust-derived ignimbrites in the southern Puna Plateau. This intense magmatic activity corresponds, in agreement with geophysical data in this region, to a process of lithospheric delamination, which allows the uprising of asthenosphere and is responsible for partial melting in the lithospheric mantle and continental crust. The primitive isotopic characteristics of Antilla rocks suggest that Antilla lavas were erupted at the margins of this zone and did not interact with crustal melts. In this scenario, the Antilla volcanism could represent the surface expression of the easternmost limit of the area affected by foundering of deep lithospheric portions.

A revision of backarc magmatic activity from the Miocene to Quaternary between 24°S and 27°S indicates that mafic magma production and eruption are most marked at around 25°S–26°S, with a high density of volcanic centers and an acme of activity at 4–5 Ma. This could be put in relation with the tectonic regime. At ~24°S, after 10 Ma, the regime was mainly compressive due to the underthrusting of the Brazilian Shield under the Andes, whereas at 25°S–26°S, after 7 Ma, the tectonic regime was mainly extensional due to a change in the tectonic stress conditions, favoring magma ascent on a relatively wider area. The location of the Antilla volcanics at the intersection of the Archibarca-Galan lineament and the Tucúman transfer zone highlights the importance of the interaction between these two large regional structures.

APPENDIX

Geochronological Methods

The geochronological study was carried out preparing the groundmass from selected fresh samples following the methods detailed in Guillou et al. (1998). The groundmass is assumed to have formed shortly after eruption and should not contain any significant excess argon. All the samples were crushed and sieved to 0.250–0.125-mm-size fractions and ultrasonically washed in acetic acid (1 *N*) for 45 min at a temperature of 60 °C to remove any secondary mineral phases that might be present in minute amounts. Phenocrysts and xenocrysts, which are potential carriers of extraneous ^{40}Ar (including excess and inherited components), were filtered out using magnetic, gravimetric, and visual handpicking separation. All the samples were dated using the unspiked K-Ar technique described by Charbit et al. (1998). When compared to the $^{40}Ar/^{39}Ar$ method, this alternative method of conventional K-Ar dating has proven successful in dating subaerial volcanic rocks (Guillou et al., 2004; Ackert et al., 2003; Singer et al., 2004; Guillou et al., 2010). This technique differs from the conventional isotope-dilution method in that argon extracted from the sample is measured in sequence with purified aliquots of atmospheric argon at the same working gas pressure in the mass spectrometer. This allows mass discrimination effects between the atmospheric reference and the unknown to be suppressed, and allows amounts of radiogenic $^{40}Ar^*$ as small as 0.14% to be detected on a single-run basis (Scaillet and Guillou, 2004). The mass spectrometer sensitivity is 5.7×10^{-3} mol/A at m/e = 40 with amplifier backgrounds of 75×10^{-12} A at m/e = 40 (10^9 ohm resistor), and $5.75\ 10^{-14}$ A at m/e = 36 (10^{11} ohm resistor). The determination of K was carried out by atomic absorption with a relative precision of 1%. Argon was extracted by radio frequency heating of a 0.5–1.0 g sample in an ultrahigh-vacuum glass line and purified with Ti sponge and Zr-Al getters. Isotopic analyses were performed on total ^{40}Ar contents ranging between 2.0×10^{-11} and 2.0×10^{-10} moles using a 180°, 6-cm-radius mass spectrometer with an accelerating potential of 620 V. The spectrometer was operated in static mode, but its volume was varied to give equal ^{40}Ar signals for the air aliquots and the samples. Beam sizes were measured simultaneously on a double Faraday collector in sets of 100 online acquisitions with a 1 s integration time. The atmospheric correction was monitored via separate measurements of atmospheric argon for each sample. Periodic cross-calibration of zero-age standards precisely constrained the mass discrimination to within ±0.5‰ on the $^{40}Ar/^{36}Ar$ ratios (Scaillet and Guillou, 2004). A manometrically calibrated dose of atmospheric argon was used to convert beam intensities into atomic abundances. This manometric calibration is based on periodic, replicate determinations of international dating standards of known K-Ar age using the same procedure for the unknowns as described in Charbit et al. (1998). This allows the total ^{40}Ar content of the sample to be determined with a precision of about ±0.2% (2σ). Standards used include LP-6 (127.8 ± 0.7 Ma; Odin, 1982, 1995) and HD-B1 (24.21 ± 0.32 Ma; Fuhrmann et al., 1987; Hess and Lippolt, 1994; Hautmann and Lippolt, 2000). At the 95% confidence level, the values adopted here are consistent with those obtained for several $^{40}Ar/^{39}Ar$ standards through the intercalibration against biotite GA-1550 by Renne et al. (1998) and Spell and McDougall (2003). Uncertainties for the K and Ar data are 1σ analytical only, and consist of propagated and quadratically averaged experimental uncertainties arising from the K, ^{40}Ar (total), and $^{40}Ar^*$ determinations. Uncertainties on the ages are given at 2σ.

In principle, the most critical uncertainty in the K-Ar method derives from the fact that it is not possible to verify the isotopic composition of the initial argon in the sample. That is, we cannot check the assumption that, at the time of its formation, its $^{40}Ar/^{36}Ar$ ratio was the modern atmospheric value (295.5). As a result, the analytical errors given in Table 2 may in principle be smaller than the true error.

ACKNOWLEDGMENTS

This work was carried out in the framework of the scientific convention between Pisa (Italy) and Salta (Argentina) Universities. The research was supported by the Consejo Nacional de Investigaciones Cientificas y Técnicas (CONICET, Argentina, grant 5341) and Consejo de Investigaciones de la Universidad Nacional de Salta (CIUNSA, Argentina, grant 20/D-249). The authors thank two anonymous reviewers for their insightful comments and J. Pelletier for the editorial handling.

REFERENCES CITED

Aceñolaza, F.G., 1992, El Sistema Ordovícico de Latinoamérica, *in* Gutiérrez Marco, J., Saavedra, J., and Rábano, I., eds., El Paleozoico Inferior de Iberoamérica: Caceres, Spain, Publicación de la Universidad de Extremadura, p. 85–118.

Aceñolaza, F.G., and Sprechmann, P., 2002, The Miocene marine transgression in the meridional Atlantic of South America: Neues Jahrbuch für Geologie und Palaontologie, Abhandlungen, v. 225, p. 75–84.

Ackert, R.A., Singer, B., Guillou, H., Kaplan, M.R., and Kurz, M.D., 2003, Cosmogenic ^{3}He production rates from $^{40}Ar/^{39}Ar$ and K-Ar dated Patagonian lava flows at 47°S: Earth and Planetary Science Letters, v. 210, p. 119–136, doi: 10.1016/S0012-821X(03)00134-1.

Acocella, V., Vezzoli, L., Omarini, R., Matteini, M., and Mazzuoli, R., 2007, Kinematic variations across Eastern Cordillera of Central Andes (24°S): Tectonic and magmatic implications: Tectonophysics, v. 434, p. 81–92, doi: 10.1016/j.tecto.2007.02.001.

Allmendinger, R.W., 1984, Estructuras transversales de la zona de transicion entre 26° y 27° S, Provincias de Tucumen y Catamarca, Argentina: Resultados preliminaries, *in* IX Congreso Geologico Argentino: Bariloche, Actas, v. 2, p. 31–47.

Allmendinger, R.W., 1986, Tectonic development, southeastern border of the Puna Plateau, northwest Argentine Andes: Geological Society of America Bulletin, v. 97, p. 1070–1082, doi: 10.1130/0016-7606(1986)97<1070:TDSBOT>2.0.CO;2.

Allmendinger, R.W., Ramos, V., Jordan, T., Palma, M., and Isacks, B.L., 1983, Paleogeography and Andean structural geometry, northwestern Argentina: Tectonics, v. 2, p. 1–16, doi: 10.1029/TC002i001p00001.

Allmendinger, R.W., Strecker, M.R., Eremchuk, J.E., and Francis, P., 1989, Neotectonic deformation of the southern Puna Plateau, northwestern Argentina: Journal of South American Earth Sciences, v. 2, p. 111–130, doi: 10.1016/0895-9811(89)90040-0.

Allmendinger, R.W., Jordan, T.E., Kay, S.M., and Isacks, B.L., 1997, The evolution of the Altiplano–Puna Plateau of the Central Andes: Annual Review of Earth and Planetary Sciences, v. 25, p. 139–174, doi: 10.1146/annurev.earth.25.1.139.

Asch, G., Schurr, B., Bohm, M., Yuan, X., Haberland, C., Heit, B., Kind, R., Woelbern, I., Bataille, K., Comte, D., Pardo, M., Viramonte, J., Rietbrock, A., and Giese, P., 2006, Seismological studies of the Central and Southern Andes, *in* Oncken, O., et al., eds., The Andes—Active Subduction Orogeny: Berlin, Springer, p. 443–457.

Assumpção, M., and Araujo, M., 1993, Effect of the Altiplano–Puna Plateau, South America, on the regional intraplate stresses: Tectonophysics, v. 221, p. 475–496, doi: 10.1016/0040-1951(93)90174-I.

Babeyko, A.Y., and Sobolev, S.V., 2005, Quantifying different modes of the late Cenozoic shortening in the Central Andes: Geology, v. 33, p. 621–624, doi: 10.1130/G21126.1.

Beck, S.L., Zandt, G., 2002, The nature of orogenic crust in the Central Andes: Journal of Geophysical Research, v. 107, no. B10, 2230, doi: 10.1029/2000JB000124.

Bossi, G.E., 1969, Geología y estrastigrafía del sector sur del valle de Choromoro, Tucumán, Argentina: Acta Geológica Lilloana, v. 10, no. 2, p. 19–65.

Bossi, G.E., Georgieff, S.M., Gavriloff, I.J.C., and Ibañez, L.M., 2001, Cenozoic evolution of the intramontane Santa María Basin, Pampean Ranges, northwestern Argentina: Journal of South American Earth Sciences, v. 14, p. 725–734, doi: 10.1016/S0895-9811(01)00058-X.

Caelles, J.C., Clark, A.H., Farrar, E., McBride, S.L., and Quirt, S., 1971, Potassium-argon ages of porphyry copper deposits and associated rocks in the Farallón Negro–Capillitas district, Catamarca, Argentina: Economic Geology and the Bulletin of the Society of Economic Geologists, v. 66, p. 961–964.

Cahill, T., Isacks, B.L., 1992, Seismicity and shape of the subducted Nazca plate: Journal of Geophysical Research, v. 97, no. B12, p. 17,503–17,529.

Carrapa, B., Hauer, J., Schoenbohm, L., Strecker, M.R., Schmitt, A.K., Villanueva, A., and Sosa Gomez, J., 2008, Dynamics of deformation and sedimentation in the northern Sierras Pampeanas: An integrated study of the Neogene Fiambalá Basin, NW Argentina: Geological Society of America Bulletin, v. 120, p. 1518–1543, doi: 10.1130/B26111.1.

Carrera, N., and Muñoz, J.A., 2008, Thrusting evolution in the southern Cordillera Oriental (northern Argentine Andes): Constraints from growth strata: Tectonophysics, v. 459, p. 107–122, doi: 10.1016/j.tecto.2007.11.068.

Carrera, N., Munoz, J.A., Sabat, F., Mon, R., and Roca, E., 2006, The role of inversion tectonics in the structure of the Cordillera Oriental (NW Argentina Andes): Journal of Structural Geology, v. 28, p. 1921–1932, doi: 10.1016/j.jsg.2006.07.006.

Charbit, S., Guillou, H., and Turpin, L., 1998, Cross calibration of K-Ar standard minerals using an unspiked Ar measurement technique: Chemical Geology, v. 150, p. 147–159, doi: 10.1016/S0009-2541(98)00049-7.

Chernicoff, C.J., Richards, J.P., and Zappettini, E.O., 2002, Crustal lineament control on magmatism and mineralization in northwestern Argentina: Geological, geophysical, and remote sensing evidence: Ore Geology Reviews, v. 21, p. 127–155.

Cladouhos, T.T., Allmendinger, R.W., Coira, B., and Farrar, E., 1994, Late Cenozoic deformation in the Central Andes: Fault kinematics from the northern Puna, northwest Argentina and southern Bolivia: Journal of South American Earth Sciences, v. 7, p. 209–228, doi: 10.1016/0895-9811(94)90008-6.

Coira, B., and Kay, S.M., 1993, Implications of Quaternary volcanism at Cerro Tuzgle for crustal and mantle evolution of the Puna Plateau, Central Andes, Argentina: Contributions to Mineralogy and Petrology, v. 113, p. 40–58, doi: 10.1007/BF00320830.

Coira, B., and Pezzutti, N., 1976, Vulcanismo Cenozoico en el ambito de Puna Catemarquena: Revista de la Asociación Geológica Argentina, v. 31, no. 1, p. 33–52.

Coira, B., Davidson, J., Mpodozis, C., and Ramos, V.A., 1982, Tectonic and magmatic evolution of the Andes of northern Argentina and Chile: Earth-Science Reviews, v. 18, p. 303–332, doi: 10.1016/0012-8252(82)90042-3.

Coira, B., Kay, S.M., and Viramonte, J., 1993, Upper Cenozoic magmatic evolution of the Argentine Puna: A model for changing subduction geometry: International Geology Review, v. 35, p. 677–720, doi: 10.1080/00206819309465552.

Coughlin, T.J., O'Sullivan, P.B., Kohn, B.P., and Holcombe, R.J., 1998, Apatite fission-track thermochronology of the Sierras Pampeanas, central western Argentina: Implications for the mechanism of plateau uplift in the Andes: Geology, v. 26, p. 999–1002, doi: 10.1130/0091-7613(1998)026<0999:AFTTOT>2.3.CO;2.

Coutand, I., Cobbold, P.R., de Urreiztieta, M., Gautier, P., Chauvin, A., Gapais, D., Rossello, E.A., and Lopez-Gamundi, O., 2001, Style and history of Andean deformation, Puna Plateau, northwestern Argentina: Tectonics, v. 20, p. 210–234, doi: 10.1029/2000TC900031.

Coutand, I., Carrapa, B., Deeken, A., Schmitt, A.K., Sobel, E.R., and Strecker, M.R., 2006, Propagation of orographic barriers along an active range front: Insights from sandstone petrography and detrital apatite fission-track thermochronology in the intramontane Angastaco Basin, NW Argentina: Basin Research, v. 18, p. 1–26, doi: 10.1111/j.1365-2117.2006.00283.x.

Cristallini, E., Cominguez, A.H., and Ramos, V.A., 1997, Deep structure of the Metan-Guachipas region: Tectonic inversion in northwestern Argentina: Journal of South American Earth Sciences, v. 10, p. 403–421, doi: 10.1016/S0895-9811(97)00026-6.

Davidson, J.P., and de Silva, S.L., 1995, Late Cenozoic magmatism of the Bolivian Altiplano: Contributions to Mineralogy and Petrology, v. 119, p. 387–408, doi: 10.1007/BF00286937.

Deeken, A., Sobel, E.R., Coutand, I., Haschke, M., Riller, U., and Strecker, M.R., 2006, Development of the southern Eastern Cordillera, NW Argentina, constrained by apatite fission track thermochronology: From Early Cretaceous extension to middle Miocene shortening: Tectonics, v. 25, TC6003, doi: 10.1029/2005TC001894.

de Silva, S.L., 1989, Altiplano-Puna volcanic complex of the Central Andes: Geology, v. 17, p. 1102–1106, doi: 10.1130/0091-7613(1989)017<1102:APVCOT>2.3.CO;2.

de Silva, S.L., Zandt, G., Trumbull, R., and Viramonte, J., 2006, Large scale silicic volcanism: The result of thermal maturation of the crust, *in* Chen Yun-tai, ed., Advances in Geosciences: River Edge, New Jersey, World Scientific Press, Proceedings of the Asia-Oceania Geosciences Society, p. 215–230.

de Urreiztieta, M., Gapais, D., Le Corre, C., Cobbold, P.R., and Rossello, E., 1996, Cenozoic dextral transpression and basin development at the southern edge of the Puna Plateau, northwestern Argentina: Tectonophysics, v. 254, p. 17–39, doi: 10.1016/0040-1951(95)00071-2.

Drew, S.T., Ducea, M.N., and Schoenbohm, L.M., 2009, Mafic volcanism on the Puna Plateau, NW Argentina: Implications for lithospheric composition and evolution with an emphasis on lithospheric foundering: Lithosphere, v. 1, p. 305–318, doi: 10.1130/L54.1.

Francis, P.W., Thorpe, R.S., Moorbath, S., Kretzschmar, G.A., and Hammill, M., 1980, Strontium isotope evidence for crustal contamination of calk-alkaline volcanic rocks from Cerro Galan, northwest Argentina: Earth and Planetary Science Letters, v. 48, p. 257–267, doi: 10.1016/0012-821X(80)90189-2.

Francis, P.W., O'Callaghan, L., Kretzschmar, G.A., Thorpe, R.S., Sparks, R.S.J., Page, R.N., de Barrio, R.E., Gillou, G., and Gonzalez, O.E., 1983, The Cerro Galan ignimbrite: Nature, v. 301, p. 51–53, doi: 10.1038/301051a0.

Francis, P.W., Sparks, R.S.J., Hawkesworth, C.J., Thorpe, R.S., and Pyle, D.M., 1989, Petrology and geochemistry of volcanic rocks of the Cerro Galan, northwest Argentina: Geological Magazine, v. 126, p. 515–547, doi: 10.1017/S0016756800022834.

Fuhrmann, U., Lippolt, H., and Hess, J.C., 1987, HD-B1 biotite reference material for K-Ar chronometry: Chemical Geology, v. 66, p. 41–51.

Galli, C.I., and Hernández, R.M., 1999, Evolution de la cuenca de antepais desde la zona de la Cumbre Calchaqui hasta la Sierra de Santa Barbara, Eocene inferior–Mioceno medio, provincia de Salta, Argentina: Acta Geologica Hispanica, v. 34, p. 167–184.

Gebhard, J.A., Guidice, A., and Gascon, J.O., 1974, Geologia de la comarca entre el Rio Juramento y Arroyo las Tortugas, provincias de Salta y Jujuy, Republica Argentina: Revista de la Asociación Geológica Argentina, v. 29, p. 359–375.

Gomez Omil, R.J., and Albarino, L.M., 1996, Análisis geológico petrolero del bloque Olleros sistema de Santa Bárbara, provincia de Salta, *in* XIII Congreso Geológico Argentino, v. 1, p. 27–44.

González, O.E., and Mon, R., 1996, Evolucion tectonica del extremo norte de las Sierras Pampeanas y su transicion a la Cordillera Oriental y a las Sierras Subandinas, *in* XIII Congreso Geologico Argentino, Buenos Aires, Actas, p. 149–160.

González, O.E., Ortega-Rivera, A., and Zentilli, M., 2005, Geochronologia del complejo volcanico Portezuelo Las Animas, Sierra del Aconquija, Provincias de Catamarca Y Tucúman, Argentina, *in* XVI Congreso Geologico Argentino, La Plata, Actas, p. 777–782.

Grier, M.E., Salfity, J.A., and Allmendinger, R.W., 1991, Andean reactivation of the Cretaceous Salta rift, northwestern Argentina: Journal of South American Earth Sciences, v. 4, p. 351–372, doi: 10.1016/0895-9811(91)90007-8.

Guillou, H., Carracedo, J.C., and Day, S., 1998, Dating of the Upper Pleistocene–Holocene volcanic activity of La Palma using the unspiked K-Ar technique: Journal of Volcanology and Geothermal Research, v. 86, p. 137–149, doi: 10.1016/S0377-0273(98)00074-2.

Guillou, H., Singer, B., Laj, C., Kissel, C., Scaillet, S., and Jicha, B.R., 2004, On the age of the Laschamp geomagnetic event: Earth and Planetary Science Letters, v. 227, p. 331–343, doi: 10.1016/j.epsl.2004.09.018.

Guillou, H., Van Vliet-Lanoe, B., Gudmundsson, A., and Nomade, S., 2010, New unspiked K–Ar ages of Quaternary sub-glacial and sub-aerial volcanic activity in Iceland: Quaternary Geochronology, v. 5, p. 10–19, doi: 10.1016/j.quageo.2009.08.007.

Guzmán, S., 2009, Petrología y relaciones tecto-magmáticas del complejo Pucarillas-Cerro Tipillas, Provincia de Salta [Ph.D. thesis]: Salta, Argentina, Universidad Nacional de Salta, 220 p.

Guzman, S.R., Petrinovic, I.A., and Brod, J.A., 2006, Pleistocene mafic volcanoes in the Puna-Cordillera Oriental boundary, NW Argentina: Journal of Volcanology and Geothermal Research, v. 158, p. 51–69, doi: 10.1016/j.jvolgeores.2006.04.014.

Halter, W.E., Bain, N., Becker, K., Heinrich, C.A., and Landtwing, M., 2004, From andesitic volcanism to the formation of a porphyry Cu-Au mineralizing magma chamber: The Farallón Negro volcanic complex, northwestern Argentina: Journal of Volcanology and Geothermal Research, v. 136, p. 1–30, doi: 10.1016/j.jvolgeores.2004.03.007.

Harris, A.C., Allen, C.M., and Bryan, S.E., 2004, ELA-ICP-MS U-Pb zircon geochronology of regional volcanism hosting the Bajo de la Alumbrera Cu-Au deposit: Implications for porphyry-related mineralization: Mineralium Deposita, v. 39, no. 1, p. 46–67, doi: 10.1007/s00126-003-0381-0.

Hautmann, H.J., and Lippolt, H.J., 2000, $^{40}Ar/^{39}Ar$ dating of central European K-Mn oxides; a chronological framework of supergene alteration processes during the Neogene: Chemical Geology, v. 170, p. 37–80, doi: 10.1016/S0009-2541(99)00241-7.

Hess, J.C., and Lippolt, H.J., 1994, Compilation of K-Ar measurements on HD-B1 standard biotite, *in* Odin, G.S., ed., Phanerozoic Time Scale: Bulletin de Liaison et d'Information, IUGS Subcommission of Geochronology, v. 12, p. 19–23.

Irvine, T.N., and Baragar, W.R.A., 1981, A guide to the chemical classification of the common volcanic rocks: Canadian Journal of Earth Sciences, v. 8, p. 523–548.

Jordan, T.E., and Allmendinger, R.W., 1986, The Sierras Pampeanas of Argentina: A modern analogue of Laramide deformation: American Journal of Science, v. 286, p. 737–764.

Kay, R.W., and Kay, S.M., 1993, Delamination and delamination magmatism: Tectonophysics, v. 219, p. 177–189, doi: 10.1016/0040-1951(93)90295-U.

Kay, S.M., and Coira, B.L., 2009, Shallowing and steepening subduction zones, continental lithospheric loss, magmatism, and crustal flow under the Central Andean Altiplano–Puna Plateau: Geological Society of America, Memoir 204, p. 229–259, doi: 10.1130/2009.1204(11).

Kay, S.M., Coira, B., and Viramonte, J., 1994, Young mafic backarc volcanic rocks as indicator of continental lithospheric delamination beneath Argentine Puna Plateau, Central Andes: Journal of Geophysical Research, v. 99, no. B12, p. 24,323–24,339, doi: 10.1029/94JB00896.

Kay, S.M., Coira, B., and Mpodozis, C., 1997, Southern central volcanic zone arc and backarc mafic magmas: Signals of Andean lithospheric processes (27°–25°S), *in* VIII Congreso Geologico Chileno, p. 1656–1661.

Kay, S.M., Mpodozis, C., and Coira, B., 1999, Magmatism, tectonism and mineral deposits of the Central Andes (22°–33°S), *in* Skinner, B.J., ed., Geology and Ore Deposits of the Central Andes: Society of Economic Geology Special Publication 7, p. 27–59.

Kleinert, K., and Strecker, M.R., 2001, Climate change in response to orographic barrier uplift: Paleosol and stable isotope evidence from the late Neogene Santa Maria Basin, northwestern Argentina: Geological Society of America Bulletin, v. 113, p. 728–742, doi: 10.1130/0016-7606(2001)113<0728:CCIRTO>2.0.CO;2.

Kley, J., and Monaldi, C.R., 1999, Estructura de las Sierras Subandinas y del Sistema de Santa Barbara, *in* Gonzalez Bonorino, G., Omarini, R., and Viramonte, J., eds., Geologia del Noroeste Argentino, XIV Congreso Geologico Argentino, v. 1, p. 415–425.

Kley, J., and Monaldi, C.R., 2002, Tectonic inversion in the Santa Barbara System of the central Andean foreland thrust belt, northwestern Argentina: Tectonics, v. 21, 1061, doi: 10.1029/2002TC902003.

Kley, J., Gangui, A.H., and Krüger, D., 1996, Basement-involved blind thrusting in the eastern Cordillera Oriental, southern Bolivia: Evidence from cross-sectional balancing, gravimetric and magnetotelluric data: Tectonophysics, v. 259, p. 171–184, doi: 10.1016/0040-1951(95)00067-4.

Kley, J., Monaldi, C.R., and Salfity, J.A., 1999, Along-strike segmentation of the Andean foreland: Causes and consequences: Tectonophysics, v. 301, p. 75–94, doi: 10.1016/S0040-1951(98)90223-2.

Knox, W.J., Kay, S.M., and Coira, B., 1989, Geochemical evidence of the origin of Quaternary basaltic andesites of the Puna, northwestern Argentina: Revista de la Asociación Geológica Argentina, v. 44, p. 194–206.

Koulakov, I., Sobolev, S.V., and Asch, G., 2006, P- and S-velocity images of the asthenosphere-lithosphere system in the Central Andes from local-source tomographic inversion: Geophysical Journal International, v. 167, p. 106–126, doi: 10.1111/j.1365-246X.2006.02949.x.

Kraemer, B., Adelmann, D., Alten, M., Schnurr, W., Erpenstein, K., Kiefer, E., van den Bogaard, P., and Gorler, K., 1999, Incorporation of the Paleogene foreland into the Neogene Puna Plateau: The Salar de Antofalla area, NW Argentina: Journal of South American Earth Sciences, v. 12, p. 157–182, doi: 10.1016/S0895-9811(99)00012-7.

Lucassen, F., Lewerenz, S., and Franz, G., 1999, Metamorphism, isotopic ages and composition of lower crustal granulite xenoliths from the Cretaceous Salta Rift, Argentina: Contributions to Mineralogy and Petrology, v. 134, p. 325–341, doi: 10.1007/s004100050488.

Lucassen, F., Escayola, M., and Romer, R.L., 2002, Isotopic composition of late Mesozoic basic and ultrabasic rocks from the Andes (23–32°S): Implications for the Andean mantle: Contributions to Mineralogy and Petrology, v. 143, p. 336–349.

Lucassen, F., Franz, G., and Viramonte, J., 2005, The Late Cretaceous lithospheric mantle beneath the Central Andes: Evidence from phase equilibria and composition of mantle xenoliths: Lithos, v. 82, p. 379–406, doi: 10.1016/j.lithos.2004.08.002.

Marquillas, R.A., and Salfity, J.A., 1988, Tectonic framework and correlations of the Cretaceous-Eocene Salta Group, Argentina: Berlin, Springer, Lecture Notes in Earth Science, v. 17, p. 119–136, doi: 10.1007/BFb0045170.

Marquillas, R.A., del Papa, C., and Sabino, I.F., 2005, Sedimentary aspects and paleoenvironmental evolution of a rift basin: Salta Group (Cretaceous-Paleogene), northwestern Argentina: International Journal of Earth Sciences, v. 94, p. 94–113, doi: 10.1007/s00531-004-0443-2.

Marrett, R., and Emerman, S.H., 1992, The relations between faulting and mafic magmatism in the Altiplano–Puna Plateau (Central Andes): Earth and Planetary Science Letters, v. 112, p. 53–59, doi: 10.1016/0012-821X(92)90006-H.

Marrett, R., and Strecker, M.R., 2000, Response of intracontinental deformation in the Central Andes to late Cenozoic reorganization of South American plate motions: Tectonics, v. 19, p. 452–467, doi: 10.1029/1999TC001102.

Marrett, R., Allmendinger, R.W., Alonso, R.N., and Drake, R.E., 1994, Late Cenozoic tectonic evolution of the Puna Plateau and adjacent foreland, northwestern Argentine Andes: Journal of South American Earth Sciences, v. 7, p. 179–207, doi: 10.1016/0895-9811(94)90007-8.

Matteini, M., Mazzuoli, R., Omarini, R., Cas, R., and Maas, R., 2002, Geodynamical evolution of the Central Andes at 24°S as inferred by magma composition along the Calama–Olacapato–El Toro transversal volcanic belt: Journal of Volcanology and Geothermal Research, v. 118, p. 205–228, doi: 10.1016/S0377-0273(02)00257-3.

Mazzuoli, R., Vezzoli, L., Omarini, R., Acocella, V., Gioncada, A., Matteini, M., Dini, A., Guillou, H., Hauser, N., Uttini, A., and Scaillet, S., 2008, Miocene magmatism and tectonics in the easternmost sector of the Calama–Olacapato–El Toro fault system in Central Andes at ~24°S: Insights into the evolution of the Eastern Cordillera: Geological Society of America Bulletin, v. 120, p. 1493–1517, doi: 10.1130/B26109.1.

McDonough, W.F., and Sun, S.S., 1995, The composition of the Earth: Chemical Geology, v. 120, p. 223–253, doi: 10.1016/0009-2541(94)00140-4.

McGlashan, N., Brown, L., and Kay, S., 2008, Crustal thickness in the Central Andes from teleseismically recorded depth phase precursors: Geophysical Journal International, v. 175, p. 1013–1022, doi: 10.1111/j.1365-246X.2008.03897.x.

Middlemost, E.A.K., 1980, A contribution to the nomenclature and classification of volcanic rocks: Geological Magazine, v. 117, p. 51–57, doi: 10.1017/S0016756800033094.

Mingramm, A., Russo, A., Pozzo, A., and Cazau, L.B., 1979, Sierras Subandinas, *in* Turner, J.C.M., ed., 2nd Simposio de Geología Regional Argentina: Academia Nacional de Ciencias, v. 1, p. 95–137.

Mon, R., 1976, The structure of the eastern border of the Andes in north-western Argentina: Geologische Rundschau, v. 65, p. 211–222, doi: 10.1007/BF01808464.

Mon, R., 1979, Esquema tectonico de los Andes del Norte Argentino: Revista de la Asociación Geológica Argentina, v. 34, p. 53–60.

Mon, R., 1999, Cordillera Oriental, *in* Gonzalez Bonorino, G., Omarini, R., and Viramonte, G., eds., Geologia del Noroeste Argentino, *in* Relatorio XIV Congreso Geológico Argentino, p. 426–431.

Mon, R., Gutierrez, A.A., Vergani, G., Pacheco, M.M., and Sabat, F., 2005, Estructura de la depression tectonica de Metan (Provincia de Salta), *in* Actas XVI Congreso Geologico Argentino, La Plata, p. 73–80.

Mortimer, E., Coutand, I., Schoenbohm, I., Carrapa, B., Sosa Gomez, J., Sobel, E.R., and Strecker, M.R., 2007, Fragmentation of a foreland basin in response to out-of-sequence basement uplifts and structural reactivation: El Cajon–Campo del Arenal basin: Geological Society of America Bulletin, v. 119, p. 637–653, doi: 10.1130/B25884.1.

Odin, G.S., ed., 1982, Numerical Dating in Stratigraphy: Chichester, UK, Wiley, 2 vols., 1094 p.

Odin, G.S., 1995, Toward conventions for reference materials for the Ar/Ar technique, *in* Odin, G.S., ed., Phanerozoic Time Scale: Bulletin de Liaison et d'Information, IUGS Subcommission of Geochronology, v. 13, p. 18.

Omarini, R.H., Sureda, R.J., Gotze, H.-J., Seilacher, A., and Pfluger, F., 1999, Puncoviscana folded belt in northwestern Argentina: Testimony of Late Proterozoic Rodinia fragmentation and pre-Gondwana collisional episodes: International Journal of Earth Sciences, v. 88, p. 76–97, doi: 10.1007/s005310050247.

Petrinovic, I.A., Riller, U., and Brod, J.A., 2005, The Negra Muerta volcanic complex, southern Central Andes: Geochemical characteristics and magmatic evolution of an episodically active volcanic centre: Journal of Volcanology and Geothermal Research, v. 140, p. 295–320, doi: 10.1016/j.jvolgeores.2004.09.002.

Prezzi, C.B., Gotze, H.J., and Schmidt, S., 2009, 3D density model of the Central Andes: Physics of the Earth and Planetary Interiors, v. 177, p. 217–234, doi: 10.1016/j.pepi.2009.09.004.

Ramos, V.A., and Aleman, A., 2000, Tectonic evolution of the Andes, *in* Cordani, U.G., Milani, E.J., Thomaz Filho, A., and Campos, D.A., eds., Tectonic Evolution of South America: Proceedings of the Thirty-first International Geological Congress, Rio de Janeiro, Brazil, p. 605–635.

Renne, P.R., Swisher, C.C., Deino, A.L., Karner, D.B., Owens, T.L., and DePaolo, D.J., 1998, Intercalibration of standards, absolute ages and uncertainties in $^{40}Ar/^{39}Ar$ dating: Chemical Geology, v. 145, p. 117–152, doi: 10.1016/S0009-2541(97)00159-9.

Reynolds, J.H., Idleman, B.D., Hernandez, R.M., and Naeser, C.W., 1994, Preliminary chronostratigraphic constraints on Neogene tectonic activity in the Eastern Cordillera and Santa Barbara System, Salta Province, NW Argentina: Geological Society of America Abstracts with Programs, v. 26, no. 7, p. A-503.

Reynolds, J.H., Galli, C.J., Hernandez, R.M., Idleman, B.D., Kotila, J.M., Hilliard, R.V., and Naeser, C.W., 2000, Middle Miocene tectonic development of the transition zone, Salta Province, northwest Argentina: Magnetic stratigraphy from the Metán Subgroup, Sierra de Gonzalez: Geological Society of America Bulletin, v. 112, p. 1736–1751, doi: 10.1130/0016-7606(2000)112<1736:MMTDOT>2.0.CO;2.

Richards, J.P., Ullrich, T., and Kerrich, R., 2006, The late Miocene–Quaternary Antofalla volcanic complex, southern Puna, NW Argentina: Protracted history, diverse petrology, and economic potential: Journal of Volcanology and Geothermal Research, v. 152, p. 197–239, doi: 10.1016/j.jvolgeores.2005.10.006.

Riller, U., Petrinovic, I.A., Ramelow, J., Strecker, M.R., and Oncken, O., 2001, Late Cenozoic tectonism, collapse caldera and plateau formation in the Central Andes: Earth and Planetary Science Letters, v. 188, p. 299–311, doi: 10.1016/S0012-821X(01)00333-8.

Risse, A., Trumbull, R.B., Coira, B., Kay, S.M., and van den Bogaard, P., 2008, $^{40}Ar/^{39}Ar$ geochronology of mafic volcanism in the backarc region of the southern Puna Plateau, Argentina: Journal of South American Earth Sciences, v. 26, p. 1–15, doi: 10.1016/j.jsames.2008.03.002.

Salfity, J.A., 1985, Lineamentos transversales al rumbo andino en el Noroeste Argentino, *in* Actas IV Congreso Geológico Cileno, v. 1, p. 119–137.

Sasso, A.M., and Clark, A.H., 1998, The Farallón Negro Group, northwest Argentina: Magmatic, hydrothermal, and tectonic evolution and implications for Cu-Au metallogeny in the Andean backarc: Society of Economic Geology Newsletter, v. 34, p. 6–18.

Scaillet, S., and Guillou, H., 2004, A critical evaluation of young (near-zero) K-Ar ages: Earth and Planetary Science Letters, v. 220, p. 265–275, doi: 10.1016/S0012-821X(04)00069-X.

Schnurr, W.B.W., Trumbull, R.B., Clavero, J., Hahne, K., Siebel, W., and Gardeweg, M., 2007, Twenty-five million years of silicic volcanism in the southern Central volcanic zone of the Andes: Geochemistry and magma genesis of ignimbrites from 25 to 27°S, 67 to 72°W: Journal of Volcanology and Geothermal Research, v. 166, p. 17–46, doi: 10.1016/j.jvolgeores.2007.06.005.

Schurr, B., Asch, G., Rietbrock, A., Trumbull, R., and Habeland, C., 2003, Complex patterns of fluid and melt transport in the Central Andes subduction zone revealed by attenuation tomography: Earth and Planetary Science Letters, v. 215, p. 105–119, doi: 10.1016/S0012-821X(03)00441-2.

Schurr, B., Rietbrock, A., Asch, G., Kind, R., and Oncken, O., 2006, Evidence for lithospheric detachment in the Central Andes from local earthquake tomography: Tectonophysics, v. 415, p. 203–223, doi: 10.1016/j.tecto.2005.12.007.

Siebel, W., Schnurr, W.B.W., Hahne, K., Kraemer, B., Trumbull, R.B., van den Bogaard, P., and Emmermann, R., 2001, Geochemistry and isotope systematics of small- to medium-volume Neogene–Quaternary ignimbrites in the southern Central Andes: Evidence for derivation from andesitic magma sources: Chemical Geology, v. 171, p. 213–237, doi: 10.1016/S0009-2541(00)00249-7.

Singer, B., Ackert, R.P., Jr., and Guillou, H., 2004, $^{40}Ar/^{39}Ar$ and K-Ar chronology of Pleistocene glaciation in Patagonia: Geological Society of America Bulletin, v. 116, p. 434–450, doi: 10.1130/B25177.1.

Sobel, E.R., and Strecker, M.W., 2003, Uplift, exhumation and precipitation: Tectonic and climatic control of late Cenozoic landscape evolution in the northern Sierras Pampeanas, Argentina: Basin Research, v. 15, p. 431–451, doi: 10.1046/j.1365-2117.2003.00214.x.

Sparks, R.S.J., Francis, P.W., Hamer, R.D., Pankhurst, R.J., O'Callagham, L.F., Thorpe, R.S., and Page, R., 1985, Ignimbrites of the Cerro Galan caldera, NW Argentina: Journal of Volcanology and Geothermal Research, v. 24, p. 205–248, doi: 10.1016/0377-0273(85)90071-X.

Spell, T.L., and McDougall, I., 2003, Characterization and calibration of $^{40}Ar/^{39}Ar$ dating standards: Chemical Geology, v. 198, p. 189–211, doi: 10.1016/S0009-2541(03)00005-6.

Steiger, R.H., and Jäger, E., 1977, Subcommission on geochronology: Convention on the use of decay constants in geo- and cosmochronology: Earth and Planetary Science Letters, v. 5, p. 320–324.

Strecker, M.R., Bloom, A.L., Malizia, D., Cerveny, P., Bossi, G., Bensel, C., and Villanueva, G.A., 1987, Nuevos datos neotectonicos sobre las Sierras Pampeanas septentrionales (26°–27°S), Repubblica Argentina, *in* X Congreso Geologico Argentino, San Miguel de Tucúman, Actas, p. 231–234.

Strecker, M.R., Cerveny, P., Bloom, A.L., and Malizia, D., 1989, Late Cenozoic tectonism and landscape development in the foreland of the Andes: Northern Sierras Pampeanas (26°–28° S), Argentina: Tectonics, v. 8, p. 517–534, doi: 10.1029/TC008i003p00517.

Trumbull, R.B., Wittenbrink, R., Hahne, K., Emerman, R., Büsch, W., Gerstenberger, H., and Siebel, W., 1999, Evidence for late Miocene to Recent contamination of arc andesites by crustal melts in the Chilean Andes (25–26°S) and its geodynamic implications: Journal of South American Earth Sciences, v. 12, p. 135–155, doi: 10.1016/S0895-9811(99)00011-5.

Trumbull, R.B., Riller, U., Oncken, O., Scheuber, E., Munier, K., and Hongn, F., 2006, The time-space distribution of Cenozoic arc volcanism in the Central Andes: A new data compilation and some tectonic implications, *in* Oncken, O., et al., eds., The Andes—Active Subduction Orogeny: Berlin, Springer-Verlag, p. 29–43.

Vandervoort, D.S., Jordan, T.E., Zeitler, P.K., and Alonso, R.N., 1995, Chronology of internal drainage development and uplift, southern Puna Plateau, Argentine Central Andes: Geology, v. 23, p. 145–148, doi: 10.1130/0091-7613(1995)023<0145:COIDDA>2.3.CO;2.

Vezzoli, L., Matteini, M., Hauser, N., Omarini, R., Mazzuoli, R., and Acocella, V., 2009, Non-explosive magma-water interaction in continental setting: Examples from the Miocene magmatism of the Eastern Cordillera of Central Andes: Bulletin of Volcanology, v. 71, p. 509–532, doi: 10.1007/s00445-008-0239-5.

Viramonte, J.G., Petrinovic, I.A., Galliski, M.A., and Aparicio Yague, A., 1994a, Manifestaciones volcanicas Cenozoicas de Antilla-San Lorenzo, Salta, Argentina (borde oriental de los Andes centrales del Sur), *in* VII Congreso Geologico Chileno, Conception 1994, Actas, v. 2, p. 1468–1472.

Viramonte, J.G., Reynolds, J.H., del Papa, C., and Disalvo, A., 1994b, The Corte Blanco garnetiferous tuff: A distinctive late Miocene marker bed in northwestern Argentina applied to magnetic polarity stratigraphy in the Rio Yacones, Salta Province: Earth and Planetary Science Letters, v. 121, p. 519–531, doi: 10.1016/0012-821X(94)90088-4.

Viramonte, J.G., Kay, S.M., Becchio, R., Escayola, M., and Novitski, I., 1999, Cretaceous rift related magmatism in central-western South America: Journal of South American Earth Sciences, v. 12, p. 109–121, doi: 10.1016/S0895-9811(99)00009-7.

Viramonte, J.G., Arnosio, M., Becchio, R., Van der Boogard, P., and Viramonte, J.M., 2008, Cerro Negro–San Lorenzo (Antilla) volcanic complex: The easternmost Andean subduction related or intraplate magmatism?, *in* Actas del XVII Congreso Geologico Argentino, Jujuy 2008, p. 244–245.

Whitman, D., Isacks, B.L., Chalelain, J.L., Chiu, J.M., and Perez, A., 1992, Attenuation of high-frequency seismic waves beneath the Central Andean Plateau: Journal of Geophysical Research, v. 97, p. 19,929–19,947, doi: 10.1029/92JB01748.

Whitman, D., Isacks, B.L., and Kay, S.M., 1996, Lithospheric structure and along-strike segmentation of the Central Andean Plateau: Seismic Q, magmatism, flexure, topography and tectonics: Tectonophysics, v. 259, p. 29–40, doi: 10.1016/0040-1951(95)00130-1.

Willner, A.P., 1990, División tectonometamórfica del basamento del noroeste Argentino, *in* Aceñolaza, F.G., Miller, H., and Toselli, A.J., eds., El Ciclo Pampeano en el Noroeste Argentino: Tucumán, Argentina, Instituto Miguel Lillio Serie de Correlación Geológica 4, p. 71–113.

Yuan, X., Sobolev, S.V., Kind, R., Oncken, O., Bock, G., Asch, G., Schurr, B., Graeber, F., Rudloff, A., Hanka, W., Wylegalla, K., Tibi, R., Haberland, C., Rietbrock, A., Giese, P., Wigger, P., Rower, P., Zandt, G., Beck, S.L., Wallace, T., Pardo, M., and Comte, D., 2000, Subduction and collision processes in the Central Andes constrained by converted seismic phases: Nature, v. 408, no. 6815, p. 958–961, doi: 10.1038/35050073.

Yuan, X., Sobolev, S.V., and Kind, R., 2002, Moho topography in the Central Andes and its geodynamic implications: Earth and Planetary Science Letters, v. 199, p. 389–402, doi: 10.1016/S0012-821X(02)00589-7.

Zandt, G., Velasco, A.A., and Beck, S.L., 1994, Composition and thickness of the southern Altiplano crust, Bolivia: Geology, v. 22, p. 1003–1006, doi: 10.1130/0091-7613(1994)022<1003:CATOTS>2.3.CO;2.

MANUSCRIPT RECEIVED 30 SEPTEMBER 2009
REVISED MANUSCRIPT RECEIVED 29 JANUARY 2010
MANUSCRIPT ACCEPTED 31 JANUARY 2010

Printed in the USA